The International Journal of Robotics Research
000(00):–

DOI:doi number
http://mms.sagepub.com

Exponentially Stabilizing Continuous-Time Controllers for Periodic Orbits of Hybrid Systems: Application to Bipedal Locomotion with Ground Height Variations

Kaveh Akbari Hamed[1]*, **Brian G. Buss**[2], **and Jessy W. Grizzle**[2]

[1]*Department of Mechanical Engineering, San Diego State University, San Diego, CA, USA*

[2]*Department of Electrical Engineering and Computer Science, University Michigan, Ann Arbor, MI, USA*

Abstract

This paper presents a systematic approach for the design of continuous-time controllers to robustly and exponentially stabilize periodic orbits of hybrid dynamical systems arising from bipedal walking. A parameterized family of continuous-time controllers is assumed so that (1) a periodic orbit is induced for the hybrid system, and (2) the orbit is invariant under the choice of controller parameters. Properties of the Poincaré map and its first- and second-order derivatives are used to translate the problem of exponential stabilization of the periodic orbit into a set of Bilinear Matrix Inequalities (BMIs). A BMI optimization problem is then set up to tune the parameters of the continuous-time controller so that the Jacobian of the Poincaré map has its eigenvalues in the unit circle. It is also shown how robustness against uncertainty in the switching condition of the hybrid system can be incorporated into the design problem. The power of this approach is illustrated by finding robust and stabilizing continuous-time feedback laws for walking gaits of two underactuated 3D bipedal robots.

Keywords

Nonlinear Control, Hybrid Systems, Underactuation, Bipedal Walking, Orbital Stability

1. Introduction

This paper addresses the problem of designing continuous-time controllers to robustly and exponentially stabilize periodic orbits of hybrid dynamical systems. Hybrid systems exhibit characteristics of both continuous-time and discrete-time dynamical systems and are used to model a large range of processes (Bainov and Simeonov, 1989; Ye et al., 1998; Haddad et al., 2006; Goebel et al., 2012) including power systems (Hiskens and Pai, 2000) and mechanical systems subject to impacts (Grizzle et al., 2001; Westervelt et al., 2007; Ames et al., 2009, 2007; Spong and Bullo, 2005; Manchester et al., 2011; Gregg et al., 2012; Gregg and Spong, 2008; Holm et al., 2007; Dai and Tedrake, 2012; Tedrake et al., 2004;

* Corresponding author; e-mail: kakbarihamed@mail.sdsu.edu

Akbari Hamed et al., 2012; Chevallereau et al., 2009; Sreenath et al., 2013; Grizzle et al., 2014; Hurmuzlu and Marghitu, 1994; Martin and Schmiedeler, 2014). Our motivation is to design robust stabilizing continuous-time controllers for 3D bipedal robots with high degrees of underactuation, but the results we present apply to non-hybrid as well as hybrid systems (Arnold, 1996; Haddad and Chellaboina, 2008; Parker and Chua, 1989).

The most basic tool to investigate the stability of hybrid periodic orbits is the method of Poincaré sections (Arnold, 1996; Parker and Chua, 1989; Haddad and Chellaboina, 2008; Haddad et al., 2006; Grizzle et al., 2001). In this approach, the evolution of the system on the Poincaré section, a hypersurface transversal to the periodic orbit, is described by a discrete-time system referred to as the Poincaré return map. In general, there is no closed-form expression for the Poincaré map, and this complicates the design of continuous-time controllers. Hence, stabilization of periodic orbits for hybrid systems is often achieved with multi-level feedback control architectures, in which continuous-time feedback laws are employed at the lower levels of the control scheme to create the periodic orbit. As the lower-level controllers may not ensure exponential stability of the orbit, a set of adjustable parameters is introduced to the continuous-time controllers. These parameters are then updated by higher-level event-based controllers when state trajectories cross the Poincaré section (Grizzle, 2006; Chevallereau et al., 2009; Gregg et al., 2012; Ramezani et al., 2013; Akbari Hamed and Grizzle, 2014; Sreenath et al., 2013). The event-based controllers are designed to render the Jacobian of the Poincaré map around the fixed point a Hurwitz matrix.

One drawback of achieving stability via event-based controllers is the potentially large delay between the occurrence of a disturbance and the event-based control effort. Alternative approaches attempt to achieve stability at the first level. Chevallereau et al. (2009) made use of a nonlinear optimization problem to minimize the spectral radius of the Jacobian of the Poincaré map for simultaneous design of periodic orbits and continuous-time controllers. Diehl et al. (2009) introduced a smoothed version of the spectral radius and a nonlinear optimization problem to generate maximally stable periodic orbits. This approach was employed to design parameters and optimal control inputs of a fully actuated bipedal robot with 2 degrees of freedom (DOF). Both methods require recomputation of the Jacobian matrix at each iteration of the optimization. For mechanical systems with many degrees of freedom and underactuation (such as the 3D bipedal robot ATRIAS (Ramezani et al., 2013), which has 13 DOF and 6 actuators), the cost of numerically computing the Poincaré map and its Jacobian makes these methods impractical. Other approaches make use of the moving Poincaré section analysis and transverse linearization techniques to design model-based and time (phase) varying LQR controllers for orbital stability of periodic orbits (Shiriaev et al., 2010; Manchester et al., 2011). These approaches have not been extensively evaluated on legged robots.

The contribution of this paper is to present a method based on sensitivity analysis and bilinear matrix inequalities (BMIs) to design continuous-time controllers that provide robust exponential stability of a given periodic orbit without relying on event-based controllers. The approach assumes that a family of parameterized continuous-time controllers has been designed so that (1) the periodic orbit is an integral curve of the closed-loop system and (2) the orbit is invariant under the choice of parameters in the controllers. By investigating the properties of the Poincaré map and its first- and second-order derivatives, a sensitivity analysis is presented. On the basis of the sensitivity analysis, the problems of robust and exponential stability are translated into a set of BMIs. A BMI optimization problem is then set up to tune the parameters of the continuous-time controllers. Finally, this approach is illustrated to design continuous-time controllers for two underactuated 3D bipedal robots with 8 and 13 DOF, respectively.

Hobbelen and Wisse (2007) introduced the gait sensitivity norm for the study of disturbance rejection in limit-cycle walkers. They calculated the Jacobian matrices on the Poincaré section based on typical perturbation analysis. In particular, for all initial conditions and disturbances, the approach runs the full-state model to calculate the Jacobian matrices. Their approach was demonstrated on a 2 DOF bipedal robot. The current paper provides additional results. First, a more systematic numerical approach is given to calculate the relevant Jacobian matrices. In particular, we relate the sensitivity matrices on the Poincaré section to nonlinear model using the variational equation (Parker and Chua, 1989, Appendix D). Second, we present a closed-form expression to calculate the sensitivity with respect to the ground

height during stepping down. Finally, in regards to feedback design, a systematic approach based on BMIs is presented to reduce the sensitivity of a bipedal robot to step-down or step-up disturbances.

Some of the results in this paper (namely, those illustrating exponential stabilization of periodic orbits for the 8 DOF bipedal robot) were already presented without mathematical proof in (Akbari Hamed et al., 2014). This paper extends the analysis to a broader class of systems and illustrates how to simultaneously optimize the continuous-time controller for robustness and exponential stability. In particular, motivated by the problem of stable walking on uneven ground, the sensitivity analysis is extended to model robustness of the orbit against uncertainty in the switching condition of the hybrid system. Furthermore, the approach is extended to hybrid systems with multiple continuous-time phases. Proofs of the key theorems are provided. Finally, the paper extends the earlier results for full-state stability as well as stability modulo yaw for 3D bipedal robots.

This paper is organized as follows. Section 2 presents the formal definitions related to hybrid systems and the Poincaré map. Required conditions on the periodic orbit and family of parameterized continuous-time controllers are presented to set up the sensitivity analysis. Two families of continuous-time controllers satisfying the required conditions are presented. Section 3 presents the BMI conditions to formulate an optimization problem to guarantee exponential stability. Section 4 extends the sensitivity analysis to form the modified BMI optimization problem for robust stability. Section 5 presents effective numerical approaches for the sensitivity analysis. Section 6 extends the analytical results to the hybrid models of bipedal walking and illustrates the method to design robust and stabilizing continuous-time controllers for two underactuated bipedal robots. Section 7 contains concluding remarks.

2. Sensitivity Analysis for Stabilization of Hybrid Periodic Orbits

The objective of this section is to present the sensitivity analysis for exponential stabilization of periodic orbits for hybrid systems arising from bipedal walking. The results of this section will be utilized in Sections 3 and 4 to set up the BMI optimization problems. We consider a hybrid system with one continuous-time phase as follows

$$\Sigma : \begin{cases} \dot{x} = f(x) + g(x)\, u, & x^- \notin \mathcal{S} \\ x^+ = \Delta(x^-), & x^- \in \mathcal{S}, \end{cases} \tag{1}$$

in which $x \in \mathcal{X}$ and $\mathcal{X} \subset \mathbb{R}^{n+1}$ denote the *vector of state variables* and $n+1$-dimensional *state manifold*, respectively. The continuous-time control input is represented by $u \in \mathcal{U}$, where $\mathcal{U} \subset \mathbb{R}^m$ is an open *set of admissible control values*. In addition, $f : \mathcal{X} \to \mathrm{T}\mathcal{X}$ and columns of g are smooth (i.e., $\mathcal{C}^\infty$) vector fields, in which $\mathrm{T}\mathcal{X}$ represents the *tangent bundle* of the state manifold $\mathcal{X}$. The *switching hypersurface* $\mathcal{S}$ is the n-dimensional manifold

$$\mathcal{S} := \{x \in \mathcal{X} \,|\, s(x) = 0\}, \tag{2}$$

on which the state solutions undergo a sudden jump according to the *re-initialization rule* $x^+ = \Delta(x^-)$. Here, $s : \mathcal{X} \to \mathbb{R}$ is a real-valued and $\mathcal{C}^\infty$ *switching function* which satisfies $\frac{\partial s}{\partial x}(x) \neq 0$ for all $x \in \mathcal{S}$. Moreover, $\Delta : \mathcal{X} \to \mathcal{X}$ denotes the $\mathcal{C}^\infty$ *reset map*. $x^-(t) := \lim_{\tau \nearrow t} x(\tau)$ and $x^+(t) := \lim_{\tau \searrow t} x(\tau)$ represent the left and right limits of the state trajectory $x(t)$, respectively.

2.1. Closed-Loop Hybrid Model

In this subsection, we assume that the continuous-time controller can be expressed as the following *parameterized feedback law*

$$u = \Gamma(x, \xi), \tag{3}$$

in which $\xi := (\xi_1, \cdots, \xi_p)^\top \in \Xi$ and $\Xi \subset \mathbb{R}^p$ represent the finite-dimensional *parameter vector* and *set of admissible parameters*, respectively, for some positive integer p. Moreover, $\Gamma : \mathcal{X} \times \Xi \to \mathcal{U}$ is a $\mathcal{C}^\infty$ map and "$\top$" denotes the matrix transpose. By employing the continuous-time feedback law (3), the closed-loop hybrid model is parameterized as follows

$$\Sigma_\xi^{\text{cl}} : \begin{cases} \dot{x} = f^{\text{cl}}(x, \xi), & x^- \notin \mathcal{S} \\ x^+ = \Delta(x^-, \xi), & x^- \in \mathcal{S}, \end{cases} \tag{4}$$

where the superscript "cl" stands for the closed-loop dynamics and $f^{\text{cl}}(x, \xi) := f(x) + g(x)\,\Gamma(x, \xi)$ is the closed-loop vector field. For later purposes, the unique solution of the closed-loop ordinary differential equation (ODE) $\dot{x} = f^{\text{cl}}(x, \xi)$ with the initial condition $x(0) = x_0$ is represented by $\varphi(t, x_0, \xi)$, where $t \geq 0$ belongs to the maximal interval of existence. Next, the *time-to-reset function* $T : \mathcal{X} \times \Xi \to \mathbb{R}_{\geq 0}$ is defined as the first time at which the solution $\varphi(t, x_0, \xi)$ intersects the switching manifold $\mathcal{S}$, i.e.,

$$T(x_0, \xi) := \inf \{t > 0 \,|\, \varphi(t, x_0, \xi) \in \mathcal{S}\}. \tag{5}$$

Remark 1 (Parameterized Reset Map)**.** In the closed-loop hybrid model of (4), the reset map is also parameterized by ξ. Our motivation for this is to extend the sensitivity approach for hybrid systems with multiple continuous-time phases of bipedal walking in Section 6. In particular, hybrid systems with multiple continuous-time phases can be expressed as hybrid systems with one continuous-time phase as in (4), in which the reset map Δ represents the composition of the flows for the remaining continuous-time and discrete-time phases. Consequently, Δ includes the parameters of the controllers employed during other phases (see Section 6 for more details).

2.2. Periodic Orbit Assumptions

Throughout this paper, we shall assume that the following assumptions are satisfied.

Assumption 1 (Invariant Periodic Orbit)**.** There exists a *period-one orbit* $\mathcal{O}$ for the parameterized closed-loop hybrid model (4) which is *invariant* under the choice of the parameter vector ξ. This assumption can be expressed precisely as follows:

1. There exists a *nominal* initial condition $x_0^* \in \mathcal{X} \setminus \mathcal{S}$ such that the solution of the ODE $\dot{x} = f^{\text{cl}}(x, \xi)$ with $x(0) = x_0^*$ is independent of ξ, i.e., $\frac{\partial \varphi}{\partial \xi}(t, x_0^*, \xi) = 0$ for all $t \geq 0$ and all $\xi \in \Xi$, where "$\setminus$" represents the set difference. For later purposes, this *invariant* and *nominal solution* is denoted by

$$\varphi^*(t) := \varphi(t, x_0^*, \xi), \quad t \geq 0. \tag{6}$$

2. The time-to-reset function, evaluated at the nominal initial condition $x = x_0^*$, is *bounded*, that is,

$$T(x_0^*, \xi) = T^* < \infty, \quad \forall \xi \in \Xi.$$

3. The reset map Δ satisfies the *reset invariance* condition

$$\Delta(x_f^*, \xi) = x_0^*, \quad \forall \xi \in \Xi, \tag{7}$$

i.e., $\frac{\partial \Delta}{\partial \xi}(x_f^*, \xi) = 0$ for all $\xi \in \Xi$, where

$$x_f^* := \varphi^*(T^*) \in \mathcal{S}. \tag{8}$$

The invariant periodic orbit $\mathcal{O}$ is then given by[1]

$$\mathcal{O} := \{x = \varphi^*(t) \,|\, 0 \leq t < T^*\} \tag{9}$$

for which T^* is the *fundamental period*. Assumption 1 states that $\mathcal{O}$ is a periodic orbit of the parameterized closed-loop hybrid model (4) for all $\xi \in \Xi$.

Assumption 2 (Transversality Condition)**.** The period-one orbit $\mathcal{O}$ in (9) is *transversal* to the switching manifold $\mathcal{S}$ in the sense that

$$\frac{\partial s}{\partial x}(x_f^*)\, f^{\mathrm{cl}}(x_f^*, \xi) \neq 0. \tag{10}$$

From Assumption 2, it can be concluded that the periodic orbit $\mathcal{O}$ is *not* tangent to the switching manifold $\mathcal{S}$ at the point $x = x_f^*$. In the next subsection, we will present two examples of continuous-time feedback laws satisfying Assumption 1.

2.3. Two Families of Parameterized and Continuous-Time Feedback Laws Satisfying the Invariance Assumption

This subsection presents two families of parameterized and continuous-time feedback laws satisfying the invariance condition in Assumption 1 for a given periodic orbit $\mathcal{O}$. If the hybrid system includes just one continuous-time phase, the reset map Δ in (4) is not parameterized by ξ and Item 3 of Assumption 1 is immediately satisfied. For the case of multiple continuous-time phases, Section 6 will present conditions under which Item 3 is met. Here, we check Item 1 for the examples and we assume that Item 3 is satisfied[2]. For this goal, we first present the following lemma.

Lemma 1 (Invariant Solution of the ODE)**.** *Consider the solution of the ODE $\dot{x} = f^{cl}(x, \xi)$ with $x(0) = x_0$. Then, $\frac{\partial \varphi}{\partial \xi}(t, x_0, \xi) = 0$ for all $t \geq 0$ if and only if*

$$\frac{\partial f^{cl}}{\partial \xi}(x, \xi)\Big|_{x=\varphi(t,x_0,\xi)} = 0, \quad \forall t \geq 0.$$

Proof. See Appendix A. □

From Lemma 1, one can immediately conclude that Item 1 of Assumption 1 is equivalent to

$$\begin{aligned} \frac{\partial f^{\mathrm{cl}}}{\partial \xi}(x, \xi)\Big|_{x\in\overline{\mathcal{O}}} &= \frac{\partial}{\partial \xi}\left(f(x) + g(x)\,\Gamma(x, \xi)\right)\Big|_{x\in\overline{\mathcal{O}}} \\ &= g(x)\,\frac{\partial \Gamma}{\partial \xi}(x, \xi)\Big|_{x\in\overline{\mathcal{O}}} \\ &= 0, \end{aligned} \tag{11}$$

where

$$\overline{\mathcal{O}} := \{x = \varphi^*(t) \,|\, 0 \leq t \leq T^*\} = \mathcal{O} \cup \{x_f^*\}$$

denotes the set closure of $\mathcal{O}$. Next to present the families of controllers, we assume that there is a $\mathcal{C}^\infty$ feedback law $\Gamma^*(x)$, referred to as the *feedforward term*, which generates the nominal trajectory $\varphi^*(t)$ in the sense that $\varphi^*(t)$ is the unique solution of $\dot{x} = f(x) + g(x)\,\Gamma^*(x)$. Suppose further that the following assumption is satisfied.

[1] Here, we assume that the solutions of the hybrid system (4) are right continuous.
[2] Since the orbit is given here, Item 2 is satisfied in the sense that the fundamental period of the orbit is bounded.

Assumption 3 (Phasing Variable)**.** Corresponding to the periodic orbit $\mathcal{O}$, there exists a real-valued and $\mathcal{C}^\infty$ function $\theta : \mathcal{X} \to \mathbb{R}$, referred to as the *phasing variable*, which is strictly monotonic (i.e., strictly increasing or decreasing) on the orbit $\overline{\mathcal{O}}$, that is,

$$\dot{\theta}(x) = \frac{\partial \theta}{\partial x}(x)\, f^{\mathrm{cl}}(x,\xi) \neq 0, \quad \forall x \in \overline{\mathcal{O}}.$$

Under Assumption 3, the desired evolution of the state variables on the orbit $\overline{\mathcal{O}}$ can be expressed in terms of the phasing variable θ rather than the time variable t. The phasing variable replaces time, which is a key to obtaining time-invariant controllers that realize exponential orbital stability of $\mathcal{O}$. In particular, let $\Theta(t)$ represent the time evolution of the phasing variable on $\overline{\mathcal{O}}$. Then, one can define the *desired evolution of the state variables* on $\overline{\mathcal{O}}$ in terms of θ as follows

$$x_{\mathrm{d}}(\theta) := \varphi^*(t)\Big|_{t=\Theta^{-1}(\theta)}, \tag{12}$$

in which $t = \Theta^{-1}(\theta)$ denotes the inverse of the strictly monotonic function $\theta = \Theta(t)$.

Example 1 (Feedforward and Linear State Feedback Law)**.** The first family of parameterized continuous-time controllers can be expressed as

$$\Gamma(x,\xi) := \Gamma^*(x) - K\ (x - x_{\mathrm{d}}(\theta))\,, \tag{13}$$

where $K \in \mathbb{R}^{m\times(n+1)}$ represents a *controller gain matrix* to be determined. Here, one can assume that the parameter vector ξ includes the elements of the gain matrix K, i.e., $\xi := \mathrm{vec}(K) \in \mathbb{R}^p$, in which $\mathrm{vec}(.)$ is the *vectorization operator* acting on matrices and $p := m\,(n+1)$. It can be easily shown that $\frac{\partial \Gamma}{\partial \xi}(x,\xi) = 0$ for all $x \in \overline{\mathcal{O}}$ and $\xi \in \Xi$. Hence, from (11), the feedback law (13) preserves the orbit $\mathcal{O}$ for all $\xi \in \Xi$.

Example 2 (Input-Output Linearizing Feedback Law)**.** For the second family of continuous-time controllers, a parameterized output function $y(x,\xi)$ with the property $\dim(y) = \dim(u) = m$ is defined as follows

$$y(x,\xi) := H\ (x - x_{\mathrm{d}}(\theta))\,, \tag{14}$$

in which $H \in \mathbb{R}^{m\times(n+1)}$ is the *output matrix* to be determined and parameterized by ξ as $\xi := \mathrm{vec}(H) \in \mathbb{R}^p$, and $p := m\,(n+1)$. The output function $y(x,\xi)$ in (14) vanishes on the orbit $\overline{\mathcal{O}}$ and we assume that Ξ is defined as an open subset of $\mathbb{R}^p$ such that $y(x,\xi)$ has uniform vector relative degree r with respect to u on an open neighborhood of $\overline{\mathcal{O}}$ for all $\xi \in \Xi$. The input-output linearizing controller takes the form

$$\begin{aligned}\Gamma(x,\xi) := &-\Big(L_g\, L_f^{r-1}\, y(x,\xi)\Big)^{-1}\ L_f^r\, y(x,\xi)\\ &-\Big(L_g\, L_f^{r-1}\, y(x,\xi)\Big)^{-1}\ \sum_{i=0}^{r-1} k_i\, L_f^i\, y(x,\xi)\end{aligned} \tag{15}$$

where $k_i, i = 0, 1, \cdots, r-1$ are constant scalars such that the polynomial $\lambda^r + k_{r-1}\,\lambda^{r-1} + \cdots + k_0 = 0$ is Hurwitz. Employing the feedback law (15) results in the following output dynamics

$$y^{(r)} + k_{r-1}\, y^{(r-1)} + \cdots + k_0\, y = 0, \tag{16}$$

for which the origin $(y, \dot{y}, \cdots, y^{(r-1)}) = (0, 0, \cdots, 0)$ is exponentially stable. Next, we show that $\frac{\partial \Gamma}{\partial \xi}(x,\xi) = 0$ for all $x \in \overline{\mathcal{O}}$ and $\xi \in \Xi$. To do this, we define the *parameterized zero dynamics manifold* corresponding to the output $y(x,\xi)$ as follows

$$\begin{aligned}\mathcal{Z}(\xi) := \{x \in \mathcal{X} \,|\, &y(x,\xi) = L_f\, y(x,\xi)\\ &= \cdots = L_f^{r-1}\, y(x,\xi) = 0\}\end{aligned}$$

on which the output function $y(x,\xi)$ is identically zero. The decoupling matrix $L_g\, L_f^{r-1}\, y(x,\xi)$ has full rank and is square on an open neighborhood of $\overline{\mathcal{O}}$, and hence, the control driving $y(x,\xi)$ to zero is unique on each zero dynamics manifold (Isidori, 1995, pp. 226). Furthermore, the orbit $\overline{\mathcal{O}}$ is common to all of the various zero dynamics manifolds. Hence, the control restricted to the orbit is independent of ξ.

2.4. Poincaré Return Map and Sensitivity Analysis

The objective of this subsection is to present the Poincaré return map and sensitivity analysis for exponential stabilization of the periodic orbit $\mathcal{O}$ for the closed-loop hybrid model (4). Here, the Poincaré section is taken as the switching manifold $\mathcal{S}$ and the Poincaré return map is defined as $P : \mathcal{X} \times \Xi \to \mathcal{X}$ by[3]

$$P(x,\xi) := \varphi\left(T(\Delta(x,\xi),\xi), \Delta(x,\xi),\xi\right) \tag{17}$$

which results in the following discrete-time system (see Fig. 1)

$$x[k+1] = P(x[k],\xi), \quad k = 0,1,\cdots. \tag{18}$$

The discrete-time system (18) maps the evolution of the hybrid system's state from a point on $\mathcal{S}$ back to $\mathcal{S}$. According to Assumption 1 and construction procedure (17), x_f^* is a *fixed point* of the Poincaré map P for all $\xi \in \Xi$, i.e.,

$$P(x_f^*,\xi) = x_f^*, \quad \forall \xi \in \Xi. \tag{19}$$

One immediate consequence of the invariant fixed point in (19) is that

$$\frac{\partial P}{\partial \xi}(x_f^*,\xi) = 0, \quad \forall \xi \in \Xi,$$

and hence, an event-based control action cannot be employed to modify the stability property of the periodic orbit $\mathcal{O}$ (Grizzle, 2006), (Westervelt et al., 2007, Chap. 4). Linearization of the discrete-time system (18) around the fixed point x_f^* then results in

$$\delta x[k+1] = \frac{\partial P}{\partial x}(x_f^*,\xi)\,\delta x[k], \quad k = 0,1,\cdots, \tag{20}$$

in which $\delta x[k] := x[k] - x_f^*$. In order to exponentially stabilize the periodic orbit $\mathcal{O}$, we would like to tune the constant parameter vector ξ such that the Jacobian matrix $\frac{\partial P}{\partial x}(x_f^*,\xi)$, when restricted to the *tangent space* $\mathrm{T}_{x_f^*}\mathcal{S}$, becomes Hurwitz in the sense that all of its eigenvalues lie inside the unit circle. However, in general there is no closed-form expression for the Poincaré map $P(x,\xi)$ nor for its Jacobian $\frac{\partial P}{\partial x}(x_f^*,\xi)$. Therefore the Poincaré map is usually obtained by numerical integration of the closed-loop hybrid model (4), while the Jacobian matrix $\frac{\partial P}{\partial x}(x_f^*,\xi)$ is obtained by numerical differentiation. The situation is more critical in mechanical systems with high degrees of freedom and high degrees of underactuation. For these systems, the numerical calculations are time consuming. In particular, employing nonlinear optimization algorithms to tune the parameter vector ξ would require extensive recomputation of the high dimensional Jacobian matrix at each iteration. To resolve this problem, we turn our attention to the *sensitivity analysis*. For this purpose, let $\xi^* \in \Xi$ represent a *nominal parameter vector*. By computing the Taylor series expansion of $\frac{\partial P}{\partial x}(x_f^*,\xi)$ around ξ^* for sufficiently small $\|\xi - \xi^*\|$, (20) becomes

$$\delta x[k+1] = \left(\frac{\partial P}{\partial x}(x_f^*,\xi^*) + \sum_{i=1}^{p} \frac{\partial^2 P}{\partial \xi_i \partial x}(x_f^*,\xi^*)\,\Delta\xi_i\right)\,\delta x[k], \tag{21}$$

[3] Here, the Poincaré map is considered from $\mathcal{X}$ to $\mathcal{X}$, whereas in Section 3, a set of coordinates for the tangent space $\mathrm{T}_{x_f^*}\mathcal{S}$ will be presented.

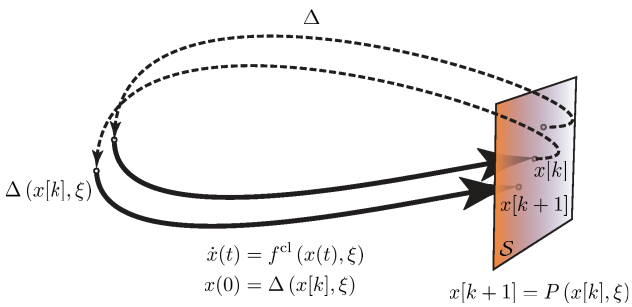

Fig. 1. Illustration of the Poincaré return map $x[k+1] = P(x[k],\xi)$ for the parameterized closed-loop hybrid model (4). The bold and dashed curves correspond to the continuous-time and discrete-time dynamics $\dot{x} = f^{\text{cl}}(x,\xi)$ and $x^+ = \Delta(x^-,\xi)$, respectively.

where $\Delta\xi := (\Delta\xi_1,\cdots,\Delta\xi_p)^\top := \xi - \xi^*$ and $\frac{\partial^2 P}{\partial\xi_i\partial x}(x_f^*,\xi^*), i = 1,\cdots,p$ are *sensitivity matrices*. The objective is to tune $\Delta\xi$ such that the origin $\delta x = 0$ becomes exponentially stable for (21). Section 3 will translate the stabilization problem into a BMI optimization problem. The robust stability problem will be addressed in Section 4. In addition, effective numerical approaches to calculate the sensitivity matrices will be presented in Section 5.

3. Translation of the Stabilization Problem into a Set of BMIs

The objective of this section is to translate the problem of exponential stabilization of the origin $\delta x = 0$ for the linearized discrete-time system (21) into a set of BMIs. To this end, we first present a set of coordinates for the tangent space $\text{T}_{x_f^*}\mathcal{S}$. In (20) and (21), the Poincaré map is considered from $\mathcal{X}$ to $\mathcal{X}$. In order to study the exponential stability behavior of the periodic orbit $\mathcal{O}$, we need to pre and post multiply the Jacobian matrix $\frac{\partial P}{\partial x}(x_f^*,\xi)$ by *constant* projection and lift matrices, respectively, to obtain a linear operator from the n-dimensional tangent space $\text{T}_{x_f^*}\mathcal{S}$ to $\text{T}_{x_f^*}\mathcal{S}$. In particular, let $\pi_{\text{proj}} \in \mathbb{R}^{n\times(n+1)}$ and $\pi_{\text{lift}} \in \mathbb{R}^{(n+1)\times n}$ denote *projection* and *lift matrices*, respectively. Next, assume that $\delta x \in \mathbb{R}^{n+1}$ is a small perturbation such that $\frac{\partial s}{\partial x}(x_f^*)\,\delta x = 0$ (this is to make sure that δx belongs to the tangent space $\text{T}_{x_f^*}\mathcal{S}$, see (2)) and let $\delta z \in \mathbb{R}^n$ be the corresponding coordinates for $\text{T}_{x_f^*}\mathcal{S}$, i.e.,

$$\begin{aligned}\delta z &= \pi_{\text{proj}}\,\delta x\\ \delta x &= \pi_{\text{lift}}\,\delta z.\end{aligned}$$

Then, from (21), the evolution of $\delta z[k], k = 0,1,\cdots$ can be expressed as

$$\delta z[k+1] = \left(A_0 + \sum_{i=1}^{p} A_i\,\Delta\xi_i\right)\,\delta z[k],\quad k = 0,1,\cdots, \tag{22}$$

where

$$\begin{aligned}A_0 &:= \pi_{\text{proj}}\,\frac{\partial P}{\partial x}(x_f^*,\xi^*)\,\pi_{\text{lift}} \in \mathbb{R}^{n\times n}\\ A_i &:= \pi_{\text{proj}}\,\frac{\partial^2 P}{\partial\xi_i\partial x}(x_f^*,\xi^*)\,\pi_{\text{lift}} \in \mathbb{R}^{n\times n},\quad i = 1,\cdots,p.\end{aligned} \tag{23}$$

Remark 2 (Properties of the Projection and Lift Matrices)**.** The projection and lift matrices have the following properties

$$\begin{aligned}&\text{(i)}\quad \pi_{\text{proj}}\,\pi_{\text{lift}} = I_{n\times n}\\ &\text{(ii)}\quad \frac{\partial s}{\partial x}(x_f^*)\,\pi_{\text{lift}} = 0.\end{aligned}$$

Next, we present the following theorem to translate the tuning of the constant perturbation vector $\Delta\xi$ for exponential stabilization of $\delta z = 0$ into a set of BMIs.

Theorem 1 (BMIs for Stabilizations of the Origin)**.** *The following statements are correct.*

1. *There exists an $n \times np$ matrix B such that*

$$A_0 + \sum_{i=1}^{p} A_i \, \Delta\xi_i = A_0 + B \, (I_{n\times n} \otimes \Delta\xi),$$

in which "$\otimes$" denotes the Kronecker product.

2. *The origin $\delta z = 0$ is exponentially stable for* (22) *if there exist $W = W^\top \in \mathbb{R}^{n\times n}$, $\Delta\xi \in \mathbb{R}^p$, and a scalar $\mu \geq 0$ such that the following BMI is satisfied*

$$\begin{bmatrix} W & A_0 \, W + B \, (I_{n\times n} \otimes \Delta\xi) \, W \\ \star & (1-\mu) \, W \end{bmatrix} > 0, \tag{24}$$

in which "$\star$" denotes the transpose of the block $(1, 2)$.

Proof. For Part 1, we claim there exists a matrix $B \in \mathbb{R}^{n\times np}$ such that for all $\Delta\xi \in \mathbb{R}^p$,

$$\sum_{i=1}^{p} A_i \, \Delta\xi_i = B \, (I_{n\times n} \otimes \Delta\xi) \, . \tag{25}$$

To show this, let us partition the B matrix as

$$B = \begin{bmatrix} B_1 & B_2 & \cdots & B_n \end{bmatrix},$$

where $B_j \in \mathbb{R}^{n\times p}$ for $j = 1, \cdots, n$. From the definition of the Kronecker product,

$$B \, (I_{n\times n} \otimes \Delta\xi) = \begin{bmatrix} B_1 & \cdots & B_n \end{bmatrix} \begin{bmatrix} \Delta\xi & \cdots & 0 \\ 0 & \cdots & 0 \\ \vdots & \ddots & \vdots \\ 0 & \cdots & \Delta\xi \end{bmatrix}.$$

Hence, the j-th column of $B \, (I_{n\times n} \otimes \Delta\xi)$ is $B_j \, \Delta\xi$ for $j = 1, \cdots, n$. To satisfy (25), one can conclude that

$$B_j \, \Delta\xi = \sum_{i=1}^{p} A_i(:, j) \, \Delta\xi_i, \tag{26}$$

where $A_i(:, j)$ represents the j-th column of A_i. Next, differentiating both sides of (26) with respect to $\Delta\xi$ together with $\frac{\partial \Delta\xi_i}{\partial \Delta\xi} = e_i^\top, i = 1, \cdots, p$ yields

$$B_j = \sum_{i=1}^{p} A_i(:, j) \, e_i^\top, \quad j = 1, \cdots, n \tag{27}$$

which completes the proof of Part 1.

For Part 2, from (24), it can be concluded that $W > 0$ and $(1-\mu)\,W > 0$ which together with $\mu \geq 0$ result in $\mu \in [0,1)$. Let us consider the Lyapunov function $V[k] := V(\delta z[k]) := \delta z[k]^\top W^{-1}\,\delta z[k]$. Next, using Schur's Lemma,

$$\begin{aligned} W\,\left(A_0 + B\,(I_{n\times n}\otimes\Delta\xi)\right)^\top W^{-1}\,\left(A_0 + B\,(I_{n\times n}\otimes\Delta\xi)\right)\,W \\ - W < -\mu\,W. \end{aligned} \tag{28}$$

Pre and post multiplying (28) with W^{-1} yields $\Delta V[k] := V[k+1] - V[k] < -\mu\,V[k]$, and hence,

$$\|\delta z[k]\|_2 < \sqrt{\frac{\lambda_{\max}(W^{-1})}{\lambda_{\min}(W^{-1})}(1-\mu)^k}\,\|\delta z[0]\|_2 \tag{29}$$

for $k = 1, 2, \cdots$, in which $\lambda_{\min}(.)$ and $\lambda_{\max}(.)$ denote the minimum and maximum eigenvalues, respectively. □

In order to have a good approximation based on the Taylor series expansion in (21), we are interested in solutions of (24) with minimum 2-norm of $\Delta\xi$. Moreover, according to the upper bound for the discrete-time solutions in (29), we would like to maximize the convergence rate, or equivalently, minimize $1-\mu$. Hence, to tune the constant perturbation $\Delta\xi$, we set up the following BMI optimization problem

$$\begin{aligned} \min_{W,\Delta\xi,\mu,\gamma}\ & -w\,\mu + \gamma \\ \text{s.t.}\ & \begin{bmatrix} W & A_0\,W + B\,(I_{n\times n}\otimes\Delta\xi)\,W \\ \star & (1-\mu)\,W \end{bmatrix} > 0 \\ & \|\Delta\xi\|_2^2 < \gamma \\ & \mu \geq 0, \end{aligned} \tag{30}$$

in which $w > 0$ is a positive weighting factor as a *tradeoff* between improving the convergence rate and minimizing the 2-norm of $\Delta\xi$. In addition, using Schur's Lemma, $\|\Delta\xi\|_2^2 < \gamma$ can also be expressed as the following linear matrix inequality (LMI)

$$\begin{bmatrix} I_{p\times p} & \Delta\xi \\ \Delta\xi^\top & \gamma \end{bmatrix} > 0.$$

Finally, the optimization problem (30) becomes

$$\begin{aligned} \min_{W,\Delta\xi,\mu,\gamma}\ & -w\,\mu + \gamma \\ \text{s.t.}\ & \begin{bmatrix} W & A_0\,W + B\,(I_{n\times n}\otimes\Delta\xi)\,W \\ \star & (1-\mu)\,W \end{bmatrix} > 0 \\ & \begin{bmatrix} I_{p\times p} & \Delta\xi \\ \star & \gamma \end{bmatrix} > 0 \\ & \mu \geq 0. \end{aligned} \tag{31}$$

For later purposes, we remark that γ and $\sqrt{1-\mu}$ represent an upper bound for $\|\Delta\xi\|_2^2$ and an upper bound for the spectral radius of $A_0 + B(I_{n\times n}\otimes\Delta\xi)$, respectively.

4. Robust Stabilization of the Periodic Orbit as a BMI Optimization Problem

The objective of this section is to address the robust stabilization of the periodic orbit $\mathcal{O}$ against uncertainty in the switching condition of (2) as a BMI optimization problem. Our motivation for this problem comes from stable bipedal

walking over uneven ground (Manchester et al., 2011; Dai and Tedrake, 2012; Hobbelen and Wisse, 2007; Saglam and Byl, 2013). To make this precise, we assume a general form of the switching manifold in (2) and denote it by $\mathcal{S}_d$, parameterized by a scalar d, as follows

$$\mathcal{S}_d := \{x \in \mathcal{X} \,|\, s(x) = d\}\,, \tag{32}$$

in which $d \in \mathcal{D}$ and $\mathcal{D} := [-d_{\max}, d_{\max}] \subset \mathbb{R}$ denotes a closed neighborhood of the origin for some positive $d_{\max}$. One can assume that d represents the height of the ground during stepping down or stepping up in bipedal walking. In the new notation, $\mathcal{S}_0 = \mathcal{S}$, where $\mathcal{S}$ was already defined in (2) as the nominal switching manifold. In what follows, we shall consider d as a *disturbance*. Corresponding to the switching manifold $\mathcal{S}_d$, the *extended time-to-reset function* $T_e : \mathcal{X} \times \Xi \times \mathcal{D} \to \mathbb{R}_{\geq 0}$ is defined as the first time at which the solution $\varphi(t, x_0, \xi)$ intersects $\mathcal{S}_d$, i.e.,

$$T_e(x_0, \xi, d) := \inf\{t > 0 \,|\, \varphi(t, x_0, \xi) \in \mathcal{S}_d\}\,. \tag{33}$$

One immediate result of (33) is that $T_e(x_0, \xi, 0) = T(x_0, \xi)$, in which $T(x_0, \xi)$ is the nominal time-to-reset function given in (5). For models of bipedal walking on rough ground, the instantaneous impact map on the manifold $\mathcal{S}_d$, extracted based on rigid body contacts (Hurmuzlu and Marghitu, 1994), does *not* depend explicitly on the ground height d and hence, it can be given by $\Delta(x, \xi)$. Now we are in a position to present the *extended Poincaré map* $P_e : \mathcal{X} \times \Xi \times \mathcal{D} \to \mathcal{X}$ as follows

$$P_e(x, \xi, d) := \varphi\left(T_e\left(\Delta(x, \xi), \xi, d\right), \Delta(x, \xi), \xi\right), \tag{34}$$

which results in the *extended* discrete-time system

$$x[k+1] = P_e\left(x[k], \xi, d[k]\right), \quad k = 0, 1, \cdots, \tag{35}$$

in which $d[k] \in \mathcal{D}$ represents the disturbance input.

Remark 3 (Geometric Description of P_e)**.** For every $x \in \mathcal{X}$, there exists $\hat{d} \in \mathbb{R}$ such that $x \in \mathcal{S}_{\hat{d}}$. In particular, one can define $\hat{d} := s(x)$ and from the definition (33), $P_e(x, \xi, d) \in \mathcal{S}_d$. One immediate result of this fact is that for a fixed $d \in \mathcal{D}$, $P_e(., \xi, d)$ maps $\mathcal{S}_d$ to $\mathcal{S}_d$, whereas the nominal Poincaré map $P(., \xi)$ in (17) maps $\mathcal{S}_0$ to $\mathcal{S}_0$. Under Assumptions 1, x^*_f is an invariant fixed point of P_e for $d = 0$ and all $\xi \in \Xi$, i.e.,

$$P_e(x^*_f, \xi, 0) = x^*_f, \quad \forall \xi \in \Xi. \tag{36}$$

Furthermore, the extended map $P_e(., \xi, 0)$ is equal to $P(., \xi)$, that is

$$P_e(., \xi, 0) = P(., \xi), \quad \forall \xi \in \Xi. \tag{37}$$

Consistent with our perspective that d represents a disturbance, we will study the robustness of the nominal fixed point x^*_f of the undisturbed system (i.e., $d[k] = 0\ \forall\ k$).[4] According to the invariance condition in (36), linearization of (35) around $(x^*_f, \xi, 0)$ results in[5]

$$\delta x[k+1] = \frac{\partial P_e}{\partial x}(x^*_f, \xi, 0)\, \delta x[k] + \frac{\partial P_e}{\partial d}(x^*_f, \xi, 0)\, d[k]. \tag{38}$$

[4] Alternatively, one could study the behavior of (35) under a constant disturbance (i.e., $d[k] = d\ \forall\ k$), assuming that a corresponding fixed point were known.

[5] We note that from (36), $\frac{\partial P_e}{\partial \xi}(x^*_f, \xi, 0) = 0$ for all $\xi \in \Xi$.

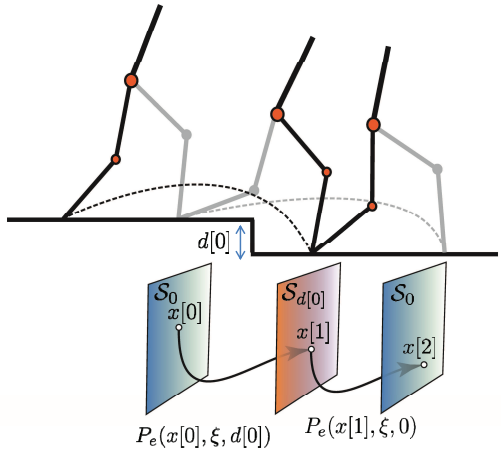

Fig. 2. Geometric description of the robustness problem for bipedal walking. Here, $x[0] = x_f^* \in \mathcal{S}_0$ and $d[0] \in \mathcal{D}$ is assumed to be a nonzero and unknown disturbance. Furthermore, $d[k] = 0$ for all $k = 1, 2, \cdots$. In this case, $x[1] = P_e(x[0], \xi, d[0]) \in \mathcal{S}_{d[0]}$ and $x[2] = P_e(x[1], \xi, 0) \in \mathcal{S}_0$. The evolution of $x[k]$ for $k = 3, 4, \cdots$ can then be described by the Poincaré return map in (18). The objective is to find $\Delta\xi$ to minimize $\|F\,\delta x[2]\|_2$ for all possible $d[0] \in \mathcal{D}$.

In this latter equation, $\delta x[k] := x[k] - x_f^*$ belongs to the $n+1$-dimensional tangent space $\mathrm{T}_{x_f^*}\mathcal{X} = \mathbb{R}^{n+1}$. Using the Taylor series expansion of $\frac{\partial P_e}{\partial x}(x_f^*, \xi, 0)$ and $\frac{\partial P_e}{\partial d}(x_f^*, \xi, 0)$ around ξ^*, (38) becomes

$$\begin{aligned}\delta x[k+1] = &\left(\frac{\partial P_e}{\partial x}(x_f^*, \xi^*, 0) + \sum_{i=1}^{p} \frac{\partial^2 P_e}{\partial \xi_i \partial x}(x_f^*, \xi^*, 0)\,\Delta\xi_i\right)\,\delta x[k] \\ &+ \left(\frac{\partial P_e}{\partial d}(x_f^*, \xi^*, 0) + \sum_{i=1}^{p} \frac{\partial^2 P_e}{\partial \xi_i \partial d}(x_f^*, \xi^*, 0)\,\Delta\xi_i\right)\,d[k].\end{aligned} \tag{39}$$

Effective numerical approaches to calculate the *extended sensitivity matrices* $\frac{\partial^2 P_e}{\partial \xi_i \partial x}(x_f^*, \xi^*, 0)$, $i = 1, \cdots, p$ will be presented in Section 5. Section 5 will also present the relation among the sensitivity matrices and extended ones. In addition, we will show that the *disturbance sensitivity matrix* $\frac{\partial P_e}{\partial d}(x_f^*, \xi, 0)$ in (38) is *independent* of ξ and hence, $\frac{\partial^2 P_e}{\partial \xi_i \partial d}(x_f^*, \xi^*, 0) = 0$. Consequently, using an analysis similar to Part 1 of Theorem 1, (39) can be rewritten as follows

$$\delta x[k+1] = \left(A_{0,e} + B_e\left(I_{(n+1)\times(n+1)} \otimes \Delta\xi\right)\right)\delta x[k] + C_e\,d[k], \tag{40}$$

in which the subscript "e" stands for the extended map and

$$A_{0,e} := \frac{\partial P_e}{\partial x}(x_f^*, \xi^*, 0) \qquad \in \mathbb{R}^{(n+1)\times(n+1)} \tag{41}$$

$$A_{i,e} := \frac{\partial^2 P_e}{\partial \xi_i \partial x}(x_f^*, \xi^*, 0) \qquad \in \mathbb{R}^{(n+1)\times(n+1)},\ i = 1, \cdots, p \tag{42}$$

$$C_e := \frac{\partial P_e}{\partial d}(x_f^*, \xi^*, 0) \qquad \in \mathbb{R}^{(n+1)\times 1} \tag{43}$$

$$B_e := \begin{bmatrix} B_{1,e} & \cdots & B_{n+1,e} \end{bmatrix} \in \mathbb{R}^{(n+1)\times(n+1)p} \tag{44}$$

$$B_{j,e} := \sum_{i=1}^{p} A_{i,e}(:, j)\,e_i^\top, \qquad j = 1, \cdots, n+1. \tag{45}$$

Now we turn our attention to the robustness problem. For this purpose, we assume that $d[0] \neq 0$ is an *unknown* disturbance and $d[k] = 0$ for $k = 1, 2, \cdots$. The initial condition is also assumed to coincide with the fixed point, i.e., $x[0] = x_f^* \in \mathcal{S}_0$. Then, from the discrete-time system (35), $x[1] \in \mathcal{S}_{d[0]}$ and $x[k] \in \mathcal{S}_0$ for $k = 2, 3, \cdots$ (see Fig. 2 as a geometric description of the problem for bipedal walking). In particular, $x[2]$ can be considered as an initial condition for the *nominal* return map P in (18). Next, the objective is to tune the constant perturbation vector $\Delta\xi$ to minimize the 2-norm of the deviation $\delta x[2] = x[2] - x_f^*$ for all possible disturbances $d[0] \in \mathcal{D}$, that is,

$$\min_{\Delta\xi} \max_{d[0]\in\mathcal{D}} \|F\,\delta x[2]\|_2, \tag{46}$$

where $F \in \mathbb{R}^{l\times(n+1)}$ is a given constant matrix.[6] From the problem statement, $\delta x[0] = 0$ and (40) result in $\delta x[1] = C_e\,d[0]$, and hence,

$$\begin{aligned}&\max_{d[0]\in\mathcal{D}} \|F\,\delta x[2]\|_2\\ &\quad= d_{\max}\,\left\|F\left(A_{0,e} + B_e\left(I_{(n+1)\times(n+1)}\otimes\Delta\xi\right)\right)C_e\right\|_2.\end{aligned}$$

Next, using Schur's Lemma, the optimization problem (46) is equivalent to the following LMI optimization

$$\begin{aligned}&\min_{\Delta\xi,\eta}\ \eta\\ &\text{s.t.}\ \begin{bmatrix} I_{l\times l} & F\left(A_{0,e} + B_e\left(I_{(n+1)\times(n+1)}\otimes\Delta\xi\right)\right)C_e\\ \star & \eta/d_{\max}^2\end{bmatrix} > 0,\end{aligned}$$

in which η is an upper bound for the *worse case* cost function $\max_{d[0]\in\mathcal{D}}\|F\,\delta x[2]\|_2$. Finally, one can combine the stabilization (see (31)) and robustness optimization problems to end up with the following BMI problem

$$\begin{aligned}&\min_{W,\Delta\xi,\mu,\gamma,\eta} -w_1\,\mu + w_2\,\eta + \gamma\\ &\text{s.t.}\\ &\begin{bmatrix} W & A_0\,W + B\,(I_{n\times n}\otimes\Delta\xi)\,W\\ \star & (1-\mu)\,W\end{bmatrix} > 0\\ &\begin{bmatrix} I_{l\times l} & F\left(A_{0,e} + B_e\left(I_{(n+1)\times(n+1)}\otimes\Delta\xi\right)\right)C_e\\ \star & \eta/d_{\max}^2\end{bmatrix} > 0\\ &\begin{bmatrix} I_{p\times p} & \Delta\xi\\ \star & \gamma\end{bmatrix} > 0\\ &\mu \geq 0,\end{aligned} \tag{47}$$

where w_1 and w_2 are positive weighting factors corresponding to the convergence rate and robustness, respectively.

5. Numerical Computation of Sensitivity Matrices

The objective of this section is to investigate the properties of the first- and second-order derivatives of the nominal and extended Poincaré maps to present effective numerical approaches to calculate the sensitivity matrices used during translating the stability and robustness problems into a set of BMIs in Sections 3 and 4.

[6] Griffin and Grizzle (2014) considered robustness to uncertainty in the impact condition during motion planning by designing the orbit so as to minimize a function of the deviation from the periodic orbit after a single step disturbance.

Sensitivity Matrices for Stability Analysis: We first present the following theorem to numerically calculate the first- and second-order Jacobian matrices in (21) for the stability analysis.

Theorem 2 (Calculation of the Sensitivity Matrices)**.** *Consider a parameterized closed-loop hybrid system as* (4) *satisfying Assumptions 1 and 2. Let*

$$\Phi(t, x_0, \xi) := \frac{\partial \varphi}{\partial x_0}(t, x_0, \xi) \in \mathbb{R}^{(n+1)\times(n+1)}$$

represent the trajectory sensitivity matrix for the closed-loop ODE $\dot{x} = f^{cl}(x, \xi)$ *and define the final value of the trajectory sensitivity matrix on the orbit* $\overline{\mathcal{O}}$ *as follows*

$$\Phi_f^*(\xi) := \Phi(T^*, x_0^*, \xi).$$

Then the Jacobian matrix of the Poincaré map, i.e., $\frac{\partial P}{\partial x}(x_f^*, \xi)$*, depends on* ξ *only through* $\Phi_f^*(\xi)$ *and* $\Upsilon(x_f^*, \xi) := \frac{\partial \Delta}{\partial x}(x_f^*, \xi)$*; i.e.,*

$$\frac{\partial P}{\partial x}(x_f^*, \xi) = \Pi(x_f^*, \xi^*)\, \Phi_f^*(\xi)\, \Upsilon(x_f^*, \xi), \quad \forall \xi \in \Xi, \tag{48}$$

in which

$$\Pi(x_f^*, \xi^*) := I_{(n+1)\times(n+1)} - \frac{f^{cl}(x_f^*, \xi^*) \frac{\partial s}{\partial x}(x_f^*)}{\frac{\partial s}{\partial x}(x_f^*) f^{cl}(x_f^*, \xi^*)}$$

is a projection matrix independent of ξ*. Furthermore, the sensitivity matrices are given by*

$$\frac{\partial^2 P}{\partial \xi_i \partial x}(x_f^*, \xi^*) = \Pi(x_f^*, \xi^*) \left\{ \frac{\partial \Phi_f^*}{\partial \xi_i}(\xi^*)\, \Upsilon(x_f^*, \xi^*) + \Phi_f^*(\xi^*)\, \frac{\partial \Upsilon}{\partial \xi_i}(x_f^*, \xi^*) \right\}, \tag{49}$$

for $i = 1, \cdots, p$*.*

Proof. See Appendix B. □

Theorem 2 simplifies the calculation of the sensitivity matrices $\frac{\partial^2 P}{\partial \xi_i \partial x}(x_f^*, \xi^*), i = 1, \cdots, p$ by relating them to the final value of the trajectory sensitivity matrix on $\overline{\mathcal{O}}$, i.e., $\Phi_f^*(\xi^*)$, and its derivatives $\frac{\partial \Phi_f^*}{\partial \xi_i}(\xi^*)$. In addition, $\Phi_f^*(\xi)$ can be obtained by numerical integration of a linear time-varying (LTV) matrix differential equation, referred to as the *variational equation* (Parker and Chua, 1989, Appendix D), as follows

$$\begin{aligned} \dot{\Phi}(t, x_0^*, \xi) &= \frac{\partial f^{\mathrm{cl}}}{\partial x}(\varphi^*(t), \xi)\, \Phi(t, x_0^*, \xi), \quad 0 \le t \le T^* \\ \Phi(0, x_0^*, \xi) &= I_{(n+1)\times(n+1)}. \end{aligned}$$

Finally, one can employ numerical differentiation approaches, like the *two point symmetric difference* method, to calculate $\frac{\partial \Phi_f^*}{\partial \xi_i}(\xi^*)$. In particular, for $i = 1, \cdots, p$,

$$\frac{\partial \Phi_f^*}{\partial \xi_i}(\xi^*) = \frac{1}{2\,\delta} \left(\Phi_f^*(\xi^* + \delta\, e_i) - \Phi_f^*(\xi^* - \delta\, e_i) \right),$$

where $\{e_1, \cdots, e_p\}$ is the standard basis for $\mathbb{R}^p$ and $\delta > 0$ is a small perturbation value.

Theorem 2 also relates the sensitivity matrices $\frac{\partial^2 P}{\partial \xi_i \partial x}(x_f^*, \xi^*), i = 1, \cdots, p$ to the sensitivity of the reset map Jacobian, i.e., $\frac{\partial \Upsilon}{\partial \xi_i}(x_f^*, \xi^*)$ (see (49)). For hybrid systems with one continuous-time phase, the reset map Δ is independent of ξ,

and hence, one can simplify (48) and (49) as follows

$$\frac{\partial P}{\partial x}(x_f^*, \xi) \quad = \Pi(x_f^*, \xi^*)\, \Phi_f^*(\xi)\, \Upsilon(x_f^*) \tag{50}$$

$$\frac{\partial^2 P}{\partial \xi_i \partial x}(x_f^*, \xi^*) = \Pi(x_f^*, \xi^*)\, \frac{\partial \Phi_f^*}{\partial \xi_i}(\xi^*)\, \Upsilon(x_f^*), \tag{51}$$

where $\Upsilon(x_f^*) := \frac{\partial \Delta}{\partial x}(x_f^*)$. The calculation of $\frac{\partial \Upsilon}{\partial \xi_i}(x_f^*, \xi^*)$ in (49) for hybrid systems with multiple continuous-time phases for bipedal walking will be addressed in Section 6 and Appendix D.

Extended Sensitivity Matrices for Robustness Analysis: The following theorem presents a numerical approach to calculate the extended sensitivity matrices as well as the disturbance sensitivity matrix in (39).

Theorem 3 (Calculation of the Extended Sensitivity Matrices)**.** *Suppose that Assumptions 1 and 2 are satisfied. Then,*

$$\frac{\partial P_e}{\partial x}(x_f^*, \xi, 0) = \frac{\partial P}{\partial x}(x_f^*, \xi) \tag{52}$$

for all $\xi \in \Xi$ which yields the following relation for the extended sensitivity matrices

$$\frac{\partial^2 P_e}{\partial \xi_i \partial x}\left(x_f^*, \xi, 0\right) = \frac{\partial^2 P}{\partial \xi_i \partial x}\left(x_f^*, \xi\right). \tag{53}$$

Furthermore, the disturbance sensitivity matrix can be expressed as

$$\frac{\partial P_e}{\partial d}(x_f^*, \xi, 0) = \frac{f^{cl}(x_f^*, \xi^*)}{\frac{\partial s}{\partial x}(x_f^*)\, f^{cl}(x_f^*, \xi^*)} \tag{54}$$

In particular, the disturbance sensitivity matrix $\frac{\partial P_e}{\partial d}(x_f^*, \xi, 0)$ is independent of ξ, i.e.,

$$\frac{\partial P_e}{\partial d}(x_f^*, \xi, 0) = \frac{\partial P_e}{\partial d}(x_f^*, \xi^*, 0). \tag{55}$$

Proof. See Appendix C. □

Finally, from Theorem 3, (23), and (42), one can conclude the following relations among the sequences $\{A_i\}$ and $\{A_{i,e}\}$

$$\begin{aligned} A_0 &= \pi_{\text{proj}}\, A_{0,e}\, \pi_{\text{lift}} \\ A_i &= \pi_{\text{proj}}\, A_{i,e}\, \pi_{\text{lift}}, \quad i = 1, \cdots, p. \end{aligned}$$

6. Application to Underactuated 3D Bipedal Robots

The objective of this section is to illustrate the sensitivity analysis and BMI optimization to systematically design robust and stabilizing continuous-time feedback laws for periodic 3D bipedal walking. Models of bipedal walking are hybrid with continuous-time phases to describe the evolution of the mechanical system according to the Euler-Lagrange equations and discrete-time phases to represent the instantaneous impacts between the swing leg end and the ground (Hurmuzlu and Marghitu, 1994). The state vector for these systems is taken as $x := (q^\top, \dot{q}^\top)^\top$, in which $q \in \mathcal{Q}$ denotes the *generalized coordinates vector* and $\mathcal{Q}$ represents the *configuration space*. The state manifold is the tangent bundle

$\mathcal{X} := \mathrm{T}\mathcal{Q}$. The hybrid model of walking includes two continuous-time phases and can be expressed as

$$\Sigma_{\mathrm{R}} : \begin{cases} \dot{x} = f_{\mathrm{R}}(x) + g_{\mathrm{R}}(x)\, u, & x^- \notin \mathcal{S}_{\mathrm{R}\to\mathrm{L}} \\ x^+ = \Delta_{\mathrm{R}\to\mathrm{L}}(x^-), & x^- \in \mathcal{S}_{\mathrm{R}\to\mathrm{L}} \end{cases}$$
$$\Sigma_{\mathrm{L}} : \begin{cases} \dot{x} = f_{\mathrm{L}}(x) + g_{\mathrm{L}}(x)\, u, & x^- \notin \mathcal{S}_{\mathrm{L}\to\mathrm{R}} \\ x^+ = \Delta_{\mathrm{L}\to\mathrm{R}}(x^-), & x^- \in \mathcal{S}_{\mathrm{L}\to\mathrm{R}}, \end{cases} \tag{56}$$

in which the subscripts "R" and "L" represent the right and left stance phases, respectively. In particular, the evolution of the robot during the stance phase $i \in \{\mathrm{R},\mathrm{L}\}$ is given by $\dot{x} = f_i(x) + g_i(x)\, u$. The right-to-left and left-to-right impact manifolds are denoted by $\mathcal{S}_{\mathrm{R}\to\mathrm{L}}$ and $\mathcal{S}_{\mathrm{L}\to\mathrm{R}}$ as follows

$$\mathcal{S}_{\mathrm{R}\to\mathrm{L}} := \{x \in \mathcal{X} \,|\, s_{\mathrm{R}\to\mathrm{L}}(x) = 0\}$$
$$\mathcal{S}_{\mathrm{L}\to\mathrm{R}} := \{x \in \mathcal{X} \,|\, s_{\mathrm{L}\to\mathrm{R}}(x) = 0\},$$

on which the right-to-left and left-to-right impacts occur, respectively. The smooth functions $s_{\mathrm{R}\to\mathrm{L}}(x)$ and $s_{\mathrm{L}\to\mathrm{R}}(x)$ represent the height of the swing leg end with respect to the ground. The right-to-left and left-to-right impacts are then given by $x^+ = \Delta_{\mathrm{R}\to\mathrm{L}}(x^-)$ and $x^+ = \Delta_{\mathrm{L}\to\mathrm{R}}(x^-)$, in which $\Delta_{\mathrm{R}\to\mathrm{L}} : \mathcal{X} \to \mathcal{X}$ and $\Delta_{\mathrm{L}\to\mathrm{R}} : \mathcal{X} \to \mathcal{X}$ are smooth impact maps (Hurmuzlu and Marghitu, 1994). Furthermore, during the continuous-time phase $i \in \{\mathrm{R},\mathrm{L}\}$, the control input u takes the form

$$u = \Gamma_i(x, \xi^i),$$

where $\Gamma_i : \mathcal{X} \times \Xi^i \to \mathcal{U}$ is a $\mathcal{C}^\infty$ state feedback law and $\xi^i \in \Xi^i$ denotes the parameter vector of phase i. The closed-loop vector field is also given by $\dot{x} = f_i^{\mathrm{cl}}(x, \xi^i) := f_i(x) + g_i(x)\, \Gamma_i(x, \xi^i)$, whose unique solution with the initial condition $x(0) = x_0$ is represented by $\varphi_i(t, x_0, \xi^i)$. The time-to-reset function during phase $i \in \{\mathrm{R},\mathrm{L}\}$ is $T_i : \mathcal{X} \times \Xi^i \to \mathbb{R}_{\geq 0}$ where

$$T_i(x_0, \xi^i) := \inf\left\{t > 0 \,|\, \varphi_i(t, x_0, \xi^i) \in \mathcal{S}_{i\to j}\right\},$$

and $j \neq i \in \{\mathrm{R},\mathrm{L}\}$. The *one-phase map* $P_{i\to j} : \mathcal{S}_{i\to j} \times \Xi^j \to \mathcal{S}_{j\to i}$, $i \neq j \in \{\mathrm{R},\mathrm{L}\}$, is defined as

$$P_{i\to j}(x, \xi^j) := \varphi_j\left(T_j\left(\Delta_{i\to j}(x), \xi^j\right), \Delta_{i\to j}(x), \xi^j\right).$$

Using (Westervelt et al., 2007, Theorem 4.3), the closed-loop hybrid model with two continuous-time phases can now be expressed in the standard form (4) as

$$\Sigma_\xi^{\mathrm{cl}} : \begin{cases} \dot{x} = f_{\mathrm{R}}^{\mathrm{cl}}(x, \xi^{\mathrm{R}}) & x^- \notin \mathcal{S}_{\mathrm{R}\to\mathrm{L}} \\ x^+ = \Delta(x^-, \xi^{\mathrm{L}}), & x^- \in \mathcal{S}_{\mathrm{R}\to\mathrm{L}}, \end{cases} \tag{57}$$

in which

$$\Delta(x, \xi^{\mathrm{L}}) := \Delta_{\mathrm{L}\to\mathrm{R}} \circ P_{\mathrm{R}\to\mathrm{L}}(x, \xi^{\mathrm{L}}) \tag{58}$$

is the composition of the left stance phase flow and the left-to-right impact map, "$\circ$" denotes the function composition, and

$$\xi := \begin{bmatrix} \xi^{\mathrm{R}} \\ \xi^{\mathrm{L}} \end{bmatrix} \in \Xi := \Xi^{\mathrm{R}} \times \Xi^{\mathrm{L}} \tag{59}$$

is the *full* parameter vector to be determined. Appendix D investigates Item 3 of Assumption 1 for the closed-loop system (57) and presents a numerical calculation approach for the sensitivity of the reset map Jacobian $\frac{\partial \Upsilon}{\partial \xi_i}(x_f^*, \xi^*), i = 1, \cdots, p$ in the sensitivity matrices (49).

6.1. Reduced-Order Sensitivity Analysis based on Left-Right Symmetry

For models of bipedal robots with left-right symmetry, the number of sensitivity matrices in the sensitivity analysis as well as the number of decision variables in the BMI optimization can be reduced significantly. The objective of this subsection is to present a systematic way for this reduced-order sensitivity analysis.

Definition 1 (Left-Right Symmetry)**.** The hybrid model of bipedal walking in (56) is said to have the *left-right symmetry* if the following conditions are satisfied.

1. $\dim(\xi^{\mathrm{R}}) = \dim(\xi^{\mathrm{L}}) = p_{\mathrm{R}}$.
2. There are *state symmetry matrix* $S_x \in \mathbb{R}^{(n+1)\times(n+1)}$ and *parameter symmetry matrix* $S_\xi \in \mathbb{R}^{p_{\mathrm{R}}\times p_{\mathrm{R}}}$ such that $S_x\, S_x = I_{(n+1)\times(n+1)}$, $S_\xi\, S_\xi = I_{p_{\mathrm{R}}\times p_{\mathrm{R}}}$, and

$$\begin{aligned} f_{\mathrm{L}}(x) &= S_x\, f_{\mathrm{R}}(S_x\, x) \\ g_{\mathrm{L}}(x)\, \Gamma_{\mathrm{L}}(x, \xi^{\mathrm{L}}) &= S_x\, g_{\mathrm{R}}(S_x\, x)\, \Gamma_{\mathrm{R}}(S_x\, x, S_\xi\, \xi^{\mathrm{L}}) \\ s_{\mathrm{L}\to\mathrm{R}}(x) &= s_{\mathrm{R}\to\mathrm{L}}(S_x\, x) \\ \Delta_{\mathrm{L}\to\mathrm{R}}(x) &= S_x\, \Delta_{\mathrm{R}\to\mathrm{L}}(S_x\, x) \end{aligned}$$

for all $x \in \mathcal{X}$ and all $\xi^{\mathrm{L}} \in \Xi^{\mathrm{L}}$.

Corresponding to the hybrid model (56), a hybrid model with one continuous-time phase was already presented in (57) whose reset map was parameterized by ξ. However, according to the symmetry (Akbari Hamed and Grizzle, 2014, Theorem 4), an alternative and equivalent hybrid model with one continuous-time phase can now be presented whose reset map is *independent* of ξ. This simplifies the sensitivity analysis as well as the BMI optimization. To make this clear, we present the following theorem.

Theorem 4 (Half Map)**.** *Assume that the hybrid model of walking has the left-right symmetry. Let $\mathcal{O} = \mathcal{O}_R \cup \mathcal{O}_L$ be a symmetric periodic orbit for the hybrid model* (56) *in the sense that $\mathcal{O}_L = S_x\, \mathcal{O}_R$. Suppose further that ξ^R and ξ^L are chosen according to the symmetry relation*

$$\xi^L = S_\xi\, \xi^R. \tag{60}$$

Then, the following statements are correct.

1. *The Poincaré return map $P : \mathcal{S}_{R\to L} \times \Xi^R \times \Xi^L \to \mathcal{S}_{R\to L}$ for the closed-loop hybrid model with two continuous-time phases can be factorized as*

$$P(x, \xi^R, \xi^L) = P_{half}\left(P_{half}\left(x, \xi^R\right), \xi^R\right),$$

in which P_{half} is the half map given by

$$P_{half}\left(x, \xi^R\right) := P_{L\to R}\left(S_x\, x, \xi^R\right). \tag{61}$$

2. *The half map is the Poincaré return map for the following hybrid system with one continuous-time phase*

$$\Sigma_\xi^{cl} : \begin{cases} \dot{x} = f_R^{cl}(x, \xi^R) & x^- \notin \mathcal{S}_{R\to L} \\ x^+ = \Delta(x^-), & x^- \in \mathcal{S}_{R\to L}, \end{cases} \tag{62}$$

in which $\xi := \xi^R$ and $\Delta(x) := \Delta_{L\to R}(S_x\, x)$ is independent of ξ.

Proof. The proof is immediate from the construction procedure (61) and (Akbari Hamed and Grizzle, 2014, Theorem 4). □

Remark 4 (Reduced-Order Sensitivity Analysis)**.** From Theorem 4,

$$\frac{\partial P}{\partial x}\left(x_f^*, \xi^{\mathrm{R}}, \xi^{\mathrm{L}}\right) = \left(\frac{\partial P_{\mathrm{half}}}{\partial x}\left(x_f^*, \xi^{\mathrm{R}}\right)\right)^2 \tag{63}$$

and hence, the periodic orbit $\mathcal{O}$ is exponentially stable for the hybrid model with two continuous-time phases if and only if $\mathcal{O}_{\mathrm{R}}$ is exponentially stable for (62). Consequently, one can apply the sensitivity analysis to the Jacobian matrix $\frac{\partial P_{\mathrm{half}}}{\partial x}(x_f^*, \xi^{\mathrm{R}})$ with fewer parameters rather than $\frac{\partial P}{\partial x}(x_f^*, \xi^{\mathrm{R}}, \xi^{\mathrm{L}})$. Finally, ξ^{L} can be obtained according to the symmetry relation (60).

6.2. Virtual Constraints

This subsection applies the analytical results of the paper to the *virtual constraints approach*. Virtual constraints are kinematic relations among the generalized coordinates enforced asymptotically by continuous-time feedback control (Grizzle et al., 2001; Westervelt et al., 2007, 2003; Freidovich et al., 2009; Ames, 2014; Lack et al., 2014; Ames et al., 2014; Akbari Hamed and Grizzle, 2014; Gregg and Sensinger, 2014; Gregg et al., 2014; Chevallereau et al., 2003, 2009; Sreenath et al., 2011, 2013; Morris and Grizzle, 2009; Maggiore and Consolini, 2013; Shiriaev et al., 2004). It has been shown that for mechanical systems with more than one degree of underactuation, the choice of virtual constraints affects the stability of the periodic orbit (Chevallereau et al., 2009). Chevallereau et al. (2009) showed that controlling the actuated coordinates for a five-link underactuated 3D bipedal robot cannot stabilize a periodic walking gait. Next, based on *physical intuition*, a different choice of virtual constraints was proposed to stabilize the same orbit. However, for ATRIAS, a related robot with additional degrees of freedom due to series elastic actuators, the same intuition did not lead to a stable periodic orbit (Ramezani et al., 2013). This underlines the importance of having a *systematic* method for choosing these constraints. This subsection relates the problem of choosing virtual constraints to the BMI optimization. This will be illustrated on the dynamical models of the five-link 3D bipedal robot of (Chevallereau et al., 2009) and of ATRIAS.

During phase $i \in \{\mathrm{R},\mathrm{L}\}$ of the hybrid model of walking (56), the virtual constraints are defined as the m-dimensional output function

$$y_i(q, \xi^i) := H^i \left(q - q_{\mathrm{d}}^i\left(\theta_i(q)\right)\right), \tag{64}$$

in which $m = \dim(u)$ is the control input dimension, H^i is a constant output matrix to be determined, $\xi^i := \mathrm{vec}(H^i)$, and $q_{\mathrm{d}}^i(\theta_i)$ represents the desired evolution of the generalized coordinates vector q on the orbit $\overline{\mathcal{O}}_i$ in terms of θ_i. Moreover, $\theta_i(q)$ denotes the phasing variable during phase i as a function of the configuration variables q (see Assumption 3). We note that in (64), $H^i\, q$ denotes the set of *controlled variables*, whereas $H^i\, q_{\mathrm{d}}^i(\theta_i)$ represents the desired evolution of the controlled variables on the orbit. If the output function (64) has uniform vector relative degree $r = 2$ on the periodic orbit, the continuous-time controller $\Gamma_i(x, \xi^i)$ is then taken as the input-output linearizing feedback law of Example 2.

Remark 5 (Symmetry in Virtual Constraints)**.** For mechanical models of bipedal robots, the state symmetry matrix can be expressed as $S_x = \text{block diag}\{S_q, S_q\}$, where S_q is the *position symmetry matrix*. Suppose further that S_y is an *output symmetry matrix* with the property $S_y\, S_y = I_{m\times m}$. If the output functions and phasing variables during the right and left stance phases are chosen such that

$$y_{\mathrm{L}}(q, \xi^{\mathrm{L}}) = S_y\, y_{\mathrm{R}}(S_q\, q, S_\xi\, \xi^{\mathrm{L}})$$
$$\theta_{\mathrm{L}}(q) = \theta_{\mathrm{R}}(S_q\, q)$$

for all $q \in \mathcal{Q}$ and $\xi^{\mathrm{L}} \in \Xi^{\mathrm{L}}$, then one can conclude that

$$H^{\mathrm{L}} = S_y\, H^{\mathrm{R}}\, S_q,$$

or equivalently, the symmetry relation (60) is satisfied[7] with $S_\xi = S_q^\top \otimes S_y$. In addition, it can be shown that all conditions of Definition 1 are satisfied[8]. Hence, we can apply the reduced-order sensitivity analysis and BMI optimization of Remark 4 to tune H^{R} (the output matrix during the right stance phase).

6.3. PENBMI Solver

In order to solve the stability and robustness BMI optimization problems in (31) and (47), we make use of the solver PENBMI[9] (TOMLAB, 2015) integrated with the MATLAB environment through the YALMIP[10] (Lofberg, 2004). BMIs are NP-hard problems (VanAntwerp and Braatz, 2000; Toker and Ozbay, 1995) however, PENBMI is a general-purpose solver for BMI optimization problems which guarantees the convergence to a critical point satisfying the first-order Karush-Kuhn-Tucker optimality conditions (Henrion et al., 2005). It is a local optimizer and its behavior (speed of convergence) depends on the initial guess. For the numerical analyses of this paper, the initial guess option for the YALMIP was not activated so that the solver looks for that. The optimization procedure for the five-link robot with 8 DOF (see Section 6.4) and ATRIAS with 13 DOF (see Section 6.6) on a computer with dual 6-core, 2.4 GHz Intel Xeon processors took approximately 20 seconds and 15 minutes, respectively.

6.4. Five-Link Walker

This subsection illustrates the results of the paper to design robust and stabilizing virtual constraints for a walking gait of an underactuated 3D bipedal robot with 8 degrees of freedom and 2 degrees of underactuation. The robot model was previously presented in (Chevallereau et al., 2009). The robot consists of a torso and two identical legs with revolute knees and point feet. Each hip has two degrees of freedom. It is assumed that there is no yaw motion about the stance leg end. Furthermore, the roll (i.e., q_1) and pitch (i.e., q_2) angles at the leg end are unactuated, whereas all of the internal joints are independently actuated. The structure and configuration variables of the robot during the right stance phase are shown in Fig. 3. Here, the phasing variable is defined as the angle of the *virtual leg* connecting the stance leg end to the stance hip in the sagittal plane. A periodic orbit $\mathcal{O}$ is then designed using the motion planning algorithm of (Chevallereau et al., 2009). The virtual constraints controller of (Chevallereau et al., 2009) can stabilize the orbit. However, it cannot handle rough ground walking. To resolve this problem, the set of nominal controlled variables is taken to be simply the actuated coordinates

$$H^{\mathrm{R}*}\, q := (q_3, q_4, q_5, q_6, q_7, q_8)^\top, \tag{65}$$

in which $H^{\mathrm{R}*} \in \mathbb{R}^{6\times 8}$ is the nominal value of the H^{R} matrix. By employing this nominal output function, the dominant eigenvalues of the 15×15 Jacobian matrix of the half map become $\{-3.3475, 0.8558, -0.2064\}$, and hence, $\mathcal{O}$ is unstable. Next, we let $\xi = \mathrm{vec}(H^{\mathrm{R}}) \in \mathbb{R}^{48}$ and employ the reduced-order sensitivity analysis as given in Remark 4. The 2-norm of the extended sensitivity matrices $A_{i,e}$ versus the elements of the H^{R} matrix is depicted in Fig. 4. From this figure, the most important sensitivity matrices around the nominal output function correspond to the first column of the H^{R} matrix, which is related to the roll angle q_1. According to this observation, we reduce the dimension of the BMI optimization problem (47) by letting $\Delta\xi$ parameterizes only the first column of the H^{R} matrix, i.e., $H^{\mathrm{R}} = H^{\mathrm{R}*} + \begin{bmatrix}\Delta\xi & 0_{6\times 1} & \cdots & 0_{6\times 1}\end{bmatrix}$. For robust stability, let $v_{\mathrm{cm}} := (v_{\mathrm{cm}}^x, v_{\mathrm{cm}}^y)^\top \in \mathbb{R}^2$ denote the horizontal components of the robot's center of mass (COM) velocity expressed in the world frame. Next, the F matrix in (46) is taken as

$$F = \frac{\partial v_{\mathrm{cm}}}{\partial x}(x_f^*)$$

[7] We make use of the vectorization operator property as $\mathrm{vec}(H^{\mathrm{L}}) = \mathrm{vec}(S_y\, H^{\mathrm{R}}\, S_q) = (S_q^\top \otimes S_y)\,\mathrm{vec}(H^{\mathrm{R}})$.
[8] The proof is similar to the one of (Akbari Hamed and Grizzle, 2014, Theorem 7).
[9] http://www.penopt.com/penbmi.html
[10] http://users.isy.liu.se/johanl/yalmip/

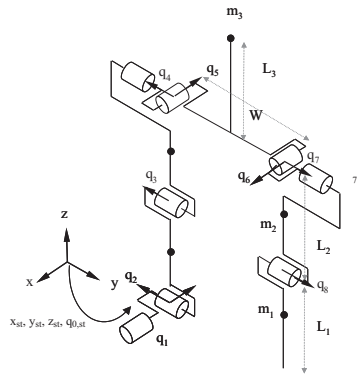

Fig. 3. A five-link 3D bipedal robot during the right stance phase with point feet and the associated configuration variables (Chevallereau et al., 2009).

to minimize the deviation in the COM velocity just before impact during uneven ground walking. Solving the optimization problem (47) with the weighting factors $w_1 = 30$ and $w_2 = 40$, and the maximum ground height variation $d_{\max} = 1(\text{cm})$ results in the following controlled variables

$$H^{\text{R}}\, q = \begin{bmatrix} q_3 + 0.4173\, q_1 \\ q_4 + 0.5094\, q_1 \\ q_5 + 0.8000\, q_1 \\ q_6 - 0.8000\, q_1 \\ q_7 + 0.2130\, q_1 \\ q_8 + 0.0966\, q_1 \end{bmatrix}. \tag{66}$$

Corresponding to this H^{R} matrix, the dominant eigenvalues of the Jacobian of the half Poincaré map, calculated based on the Taylor series expansion (21), are $\{-0.9329, 0.9341, 0.3463\}$. Next, the dominant eigenvalues of the real Jacobian of the half Poincaré map become $\{-0.9319, 0.8269, 0.5869\}$. Figure 5 depicts the phase portraits of the roll and pitch angles during 80 consecutive steps on flat ground. Here, the simulation of the closed-loop system is started off the orbit with an error of 6 (deg/s) on each component of the generalized velocity vector $\dot{q}$. Convergence to a stable limit cycle is clear.

The results of the sensitivity analysis shown in Fig. 4 and the optimized virtual constraints (66) have an important interpretation. The nominal output function

$$y(q, \xi^*) = h_0(q) - h_d(\theta_{\text{pitch}}(q)), \tag{67}$$

coordinates the links based only upon a phasing variable $\theta_{\text{pitch}}(q) = \theta(q)$ defined in the sagittal plane. Thus it ignores deviations from the periodic orbit in the roll direction. In contrast, the optimized output function, which can be expressed as[11]

$$y(q, \xi) = h_0(q) - h_d(\theta_{\text{pitch}}(q)) - \bar{h}_d(\theta_{\text{roll}}(q)), \tag{68}$$

responds to roll angle errors by adjusting the desired evolutions of the controlled variables. This new output enhances stability of the periodic orbit by coupling pitch and roll in a way that would be impossible to discover through intuition.

To evaluate the robustness of the closed-loop system for uneven ground walking, a ground height profile $d[k]$ with $d[k] \in [-d_{\max}, d_{\max}]$ is considered, in which $d_{\max} = 0.01$ (m). It is further assumed that $d[k]$ is periodic with the period of 7 steps, i.e., $d[k+7] = d[k]$ for all $k = 0, 1, \cdots$. Figure 6 presents the ground height profile $d[k]$ and corresponding

[11] Note that the term $\bar{h}_d(\theta_{\text{roll}}(q))$ vanishes on the orbit. Furthermore, the pseudo-phasing variable $\theta_{\text{roll}}(q)$ need not satisfy Assumption 3.

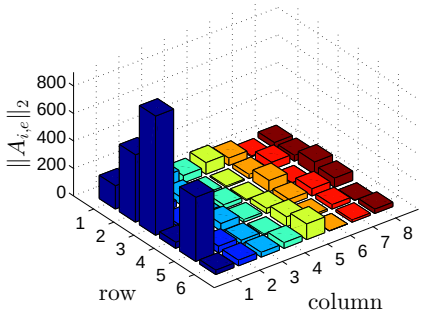

Fig. 4. Plot of the 2-norm of the extended sensitivity matrices versus the components of the 6×8 H^{R} matrix around the nominal output function. Here, $i = \text{row} + 6(\text{column} - 1)$.

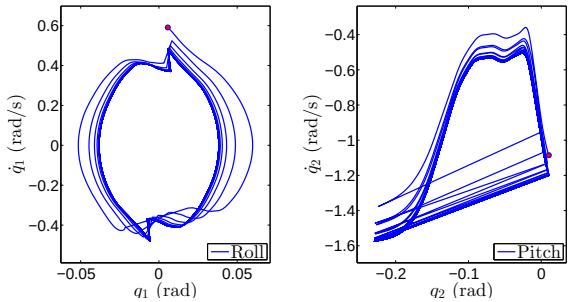

Fig. 5. Phase portraits of the closed-loop hybrid system for the roll and pitch coordinates during 80 consecutive steps of walking corresponding to the optimal solutions of (47). The circles represent the initial condition of the simulator.

x and y components of the COM velocity deviation $\delta v_{\mathrm{cm}}[k]$ for the robust optimal solution versus the step number k. The animation of this simulation can be found at (Grizzle, 2015).

6.5. Exponential Stability Modulo Yaw

The five-link walker of Subsection 6.4 does not have yaw motion about the stance leg end. For bipedal robots with yaw motion, there are two kinds of stability during walking on a flat ground: *full-state stability* and *stability modulo yaw* (Shih et al., 2012). This subsection extends the sensitivity analysis developed in Subsection 2.4 for exponential stability *modulo yaw* in 3D bipedal walking. To achieve this goal, without loss of generality, we assume that the first component of the state vector x represents the *yaw position* of the robot with respect to the world frame and we denote this component by x_{yaw}. From the *equivariance property* of (Shih et al., 2012), if the feedback laws $\Gamma_i(x, \xi^i), i \in \{\mathrm{R},\mathrm{L}\}$ do not depend on the yaw position (i.e., x_{yaw}), then the first column of the Jacobian matrix $\frac{\partial P}{\partial x}(x_f^*, \xi^{\mathrm{R}}, \xi^{\mathrm{L}})$ becomes $(1, 0, \cdots, 0)^\top$. In particular, there is an eigenvalue "1" corresponding to the yaw position. Hence, for exponential stability modulo yaw, we apply the sensitivity analysis to

$$\frac{\partial \check{P}}{\partial x}(x_f^*, \xi^{\mathrm{R}}, \xi^{\mathrm{L}}),$$

in which $\frac{\partial \check{P}}{\partial x}(x_f^*, \xi^{\mathrm{R}}, \xi^{\mathrm{L}})$ represents the $(n-1) \times (n-1)$ matrix obtained by removing the first row and column of $\frac{\partial P}{\partial x}(x_f^*, \xi^{\mathrm{R}}, \xi^{\mathrm{L}})$. This approach can also be applied to the half map developed in Theorem 4. For this goal, we assume that on the orbit $\mathcal{O}$, the symmetry condition for the yaw position can be given as

$$x_{\mathrm{yaw}}(t + T^*) = -x_{\mathrm{yaw}}(t), \quad \forall t \geq 0.$$

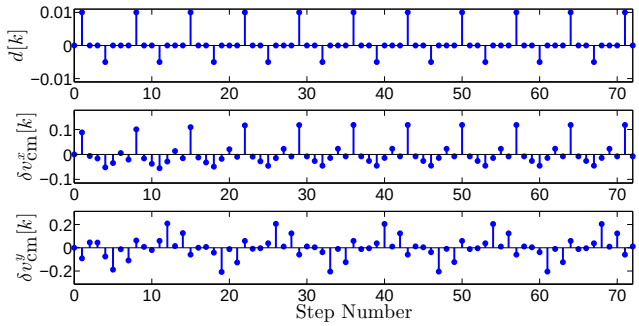

Fig. 6. Plot of a ground height profile $d[k]$ (m) and the corresponding x and y components of the deviation in the five-link robot's COM velocity (i.e., $\delta v_{\rm cm}[k]$) (m/s) for the optimal solution of (47) versus the step number k.

Then, the $(1,1)$ element of the state symmetry matrix S_x is -1, and hence, the first column of $\frac{\partial P_{\rm half}}{\partial x}(x_f^*, \xi^{\rm R})$ would be $(-1, 0, \cdots, 0)^\top$. Similarly, for exponential stability modulo yaw, one can apply the sensitivity analysis to the $(n-1)\times(n-1)$ matrix

$$\frac{\partial \check{P}_{\rm half}}{\partial x}(x_f^*, \xi^{\rm R})$$

obtained by removing the first row and column of $\frac{\partial P_{\rm half}}{\partial x}(x_f^*, \xi^{\rm R})$.

Remark 6 (Equivariance Property for Virtual Constraints)**.** In the virtual constraints approach, it can be shown that if (i) the columns corresponding to the yaw position in the output matrices H^i are zero and (ii) the phasing variables $\theta_i(q)$ do not depend on the yaw position, then the input-output linearizing feedback law (15) is independent of yaw and hence, the equivariance property of (Shih et al., 2012) is satisfied.

6.6. ATRIAS

ATRIAS 2.1 is a human scale and underactuated 3D bipedal robot with *point feet* and *series-compliant actuators*, designed for energy efficient and robust walking (Ramezani et al., 2013; ATRIAS, 2013; Grimes and Hurst, 2012) (see Fig. 7). During the single support phase, the mechanical model of the robot has 13 DOF and 6 actuators. Hence, the system is highly underactuated with 7 degrees of underactuation. The robot consists of a torso and two identical legs.

The orientation of the torso with respect to an inertial world frame can be described by three *Euler* angles $q_{z\rm T}$, $q_{y\rm T}$ and $q_{x\rm T}$, referred to as the *yaw*, *roll* and *pitch*. In the sagittal plane, the angles of the shin and thigh links with respect to the torso are denoted by $q_{1\rm R}$ and $q_{2\rm R}$ for the right leg (again see Fig. 7) and by $q_{1\rm L}$ and $q_{2\rm L}$ for the left leg. To control these angles, two DC motors in series with harmonic drives are located at each of the hips. The angles of the outputs of harmonic drives with respect to the torso are represented by $q_{gr1\rm R}$ and $q_{gr2\rm R}$ for the right leg and $q_{gr1\rm L}$ and $q_{gr2\rm L}$ for the left leg. In addition, $u_{1\rm R}$, $u_{2\rm R}$, $u_{1\rm L}$ and $u_{2\rm L}$ denote the torques generated by the corresponding DC motors. The hips are driven by two DC motors, located in the torso. In the frontal plane, the angles of the right and left hips with respect to the torso are represented by $q_{3\rm R}$ and $q_{3\rm L}$, respectively (again see Fig. 7). The generated torques by the hip motors are denoted by $u_{3\rm R}$ and $u_{3\rm L}$. Finally, the generalized coordinate vector of ATRIAS can be expressed as

$$q := (q_{z\rm T}, q_{y\rm T}, q_{x\rm T}, q_{1\rm R}, q_{2\rm R}, q_{1\rm L}, q_{2\rm L}, q_{gr1\rm R}, q_{gr2\rm R}, q_{3\rm R}, q_{gr1\rm L}, q_{gr2\rm L}, q_{3\rm L})^\top, \tag{69}$$

in which the first seven components of q are unactuated, whereas the remaining six components are actuated. The control input u is taken as the following 6-dimensional vector

$$u := (u_{1\rm R}, u_{2\rm R}, u_{3\rm R}, u_{1\rm L}, u_{2\rm L}, u_{3\rm L})^\top.$$

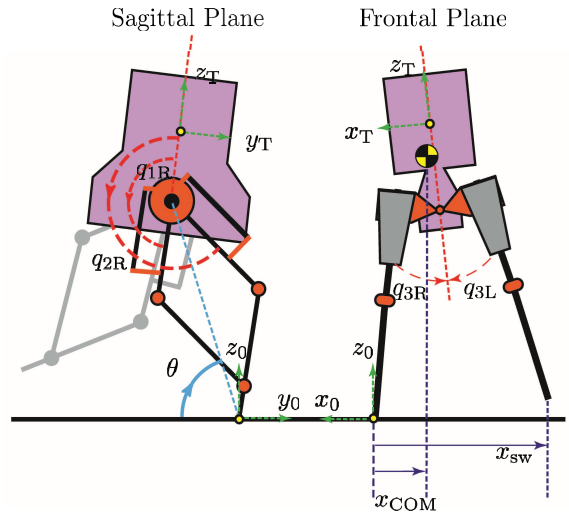

Fig. 7. Sagittal and frontal planes of ATRIAS 2.1 during the right stance phase with the associated configuration variables. The Euler angles $q_{z\mathrm{T}}$ (yaw), $q_{y\mathrm{T}}$ (roll) and $q_{x\mathrm{T}}$ (pitch) describe the rotation of the torso frame $0_{\mathrm{T}}x_{\mathrm{T}}y_{\mathrm{T}}z_{\mathrm{T}}$ with respect to the world frame $0_0x_0y_0z_0$.

Furthermore, the phasing variable is defined as the angle of the virtual leg in the sagittal plane.

In what follows, $\mathcal{O} = \mathcal{O}_{\mathrm{R}} \cup \mathcal{O}_{\mathrm{L}}$ is a periodic orbit for walking at 1.1 (m/s) designed using the motion planning algorithm of (Ramezani et al., 2013).

Stability Modulo Yaw To stabilize the periodic orbit $\mathcal{O}$ module yaw, the nominal controlled variables are taken as

$$H^{\mathrm{R}*}\, q = \begin{bmatrix} \frac{1}{2}(q_{gr1\mathrm{R}} + q_{gr2\mathrm{R}}) \\ \frac{1}{2}(q_{gr1\mathrm{L}} + q_{gr2\mathrm{L}}) \\ q_{gr2\mathrm{R}} - q_{gr1\mathrm{R}} \\ q_{gr2\mathrm{L}} - q_{gr1\mathrm{L}} \\ q_{3\mathrm{R}} \\ \frac{\partial}{\partial q}\left(x_{\mathrm{sw}} - x_{\mathrm{COM}}\right)(x_f^*)\, q \end{bmatrix}, \tag{70}$$

where the first and second components are the stance and swing leg angles, respectively. The leg angle is defined in the sagittal plane as the angle between the torso and the virtual line connecting the hip to the leg end. The third and fourth components of the controlled variables in (70) are the stance and swing knee angles, respectively. We note that since the legs are actuated through springs, the leg and knee angles have been defined at the outputs of the harmonic drives. These components can stabilize periodic orbits for planar walking of ATRIAS (Ramezani et al., 2013). The fifth component is then defined as the stance hip angle in the frontal plane. Finally, $x_{\mathrm{sw}}(q) - x_{\mathrm{COM}}(q)$ denotes the horizontal distance between the robot's COM and swing leg end in the frontal plane. Here, $x_{\mathrm{sw}}(q)$ and $x_{\mathrm{COM}}(q)$ represent the horizontal coordinates of the swing leg end and COM in the frontal plane, respectively (see Fig. 7). The sixth component of the controlled variables in (70) is taken as the linearized approximation of the distance function around the orbit $\mathcal{O}_{\mathrm{R}}$ just before the impact (i.e., x_f^*). The idea of controlling the distance between the COM and swing leg end in the frontal plane originated in (Chevallereau et al., 2009). For the five-link robot of Subsection 6.4, the distance function can stabilize the gait, whereas for the ATRIAS structure, it cannot. In particular, the dominant eigenvalues of the 25×25 Jacobian of the half Poincaré map are $\{-1.0000, -1.3011, 0.8363, -0.1602\}$. Since the distance function is defined in the frontal plane, it is yaw invariant and hence, from Remark 6, the eigenvalue -1 corresponds to the yaw position.

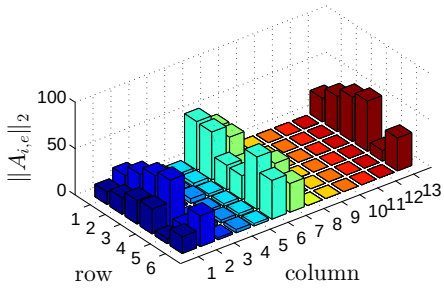

Fig. 8. Plot of the 2-norm of the extended sensitivity matrices versus the components of the 6×13 H^{R} matrix around the nominal output function (70). Here, $i = \text{row} + 6(\text{column} - 1)$.

Figure 8 represents the 2-norm of the extended sensitivity matrices versus the elements of the H^{R} matrix. From this figure, the most important sensitivity matrices relate to columns $1-7$ and 13. However, the first column corresponds to the yaw position and we do not consider it for stability modulo yaw. According to these observations, we let $\Delta\xi$ parameterize only the columns $2-7$ and 13. Next, the optimization problem (47) with $w_1 = 1$, $w_2 = 1$ and $d_{\max} = 1$ (cm) is solved for exponential and robust stability. The optimal controlled variables, i.e., $H^{\mathrm{R}}\, q$, are then given by[12]

$$\begin{bmatrix} \frac{1}{2}(q_{gr1\mathrm{R}} + q_{gr2\mathrm{R}}) \\ \frac{1}{2}(q_{gr1\mathrm{L}} + q_{gr2\mathrm{L}}) \\ q_{gr2\mathrm{R}} - q_{gr1\mathrm{R}} \\ q_{gr2\mathrm{L}} - q_{gr1\mathrm{L}} \\ q_{3\mathrm{R}} \\ \frac{\partial}{\partial q}\left(x_{\mathrm{sw}} - x_{\mathrm{COM}}\right)(x_f^*)\, q \end{bmatrix} + \begin{bmatrix} -0.1193\, q_{y\mathrm{T}} - 0.1277\, q_{3\mathrm{L}} \\ +0.0786\, q_{y\mathrm{T}} + 0.0842\, q_{3\mathrm{L}} \\ -0.0313\, q_{y\mathrm{T}} - 0.0334\, q_{3\mathrm{L}} \\ +0.0400\, q_{y\mathrm{T}} + 0.0428\, q_{3\mathrm{L}} \\ +0.0038\, q_{y\mathrm{T}} + 0.0041\, q_{3\mathrm{L}} \\ -0.2731\, q_{y\mathrm{T}} - 0.2923\, q_{3\mathrm{L}} \end{bmatrix}. \tag{71}$$

Corresponding to these controlled variables, the dominant eigenvalues of the 25×25 Jacobian of the half Poincaré map, calculated based on the Taylor series expansion (21), are $\{-1.0000, -0.9033, 0.8087, 0.5410, -0.1128\}$. For comparison, the dominant eigenvalues of the real Jacobian of the half Poincaré map become $\{-1.0000, -0.8183, 0.8686 \pm 0.1011i, -0.1104\}$. The controlled variables (71) can also be interpreted as defining a modified output of the form (68).

Figure 9 depicts the phase portraits of the closed-loop system during 50 consecutive steps of walking. Here, the simulation starts at the end of the left stance phase on the periodic orbit (see the circles in the plots). During the fourth step, an external horizontal force with a magnitude of $100(\mathrm{N})$ is applied to the COM of the robot for 50% of the step. Convergence to the periodic orbit is clear. The orbit $\mathcal{O}$ has been designed to walk along the y-axis of the world frame which corresponds to the yaw angle $q_{z\mathrm{T}}$ being zero. However, since the orbit is exponentially stable modulo yaw, the horizontal disturbance changes the direction of walking by shifting the phase portrait in the yaw coordinates.

To evaluate the robustness of the closed-loop system, we simulated walking over a periodic sequence of ground height disturbance $d[k] \in [-d_{\max}, d_{\max}]$ with the period 20. The maximum disturbance size $d_{\max} = 0.03$ (m) corresponds to 3.75% of robot's leg length. Figure 6 presents the evolutions of the disturbance $d[k]$ and corresponding x and y components of the COM velocity deviation $\delta v_{\mathrm{cm}}[k]$ for the optimal solution. An animation of this simulation can be found at (Grizzle, 2015).

Yaw Stability Next, our objective is to improve the controlled variables (71) for full exponential stability including yaw. For this goal, the sensitivity analysis is done around the improved output function (71). Figure 11 depicts the 2-norm of

[12] For this optimal solution, the elements of $\Delta\xi$ corresponding to columns $3-7$ are very small and are not reported here.

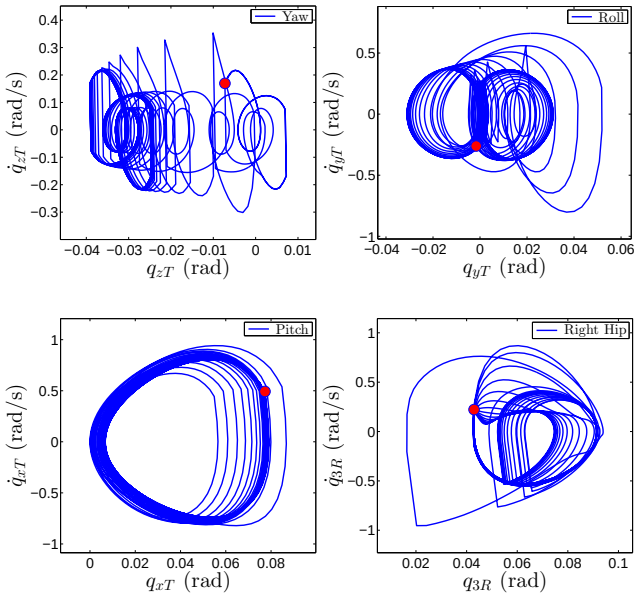

Fig. 9. Phase portraits of the closed-loop hybrid system for the Euler angles and right hip during 50 consecutive steps corresponding to the optimal solutions of (47) for stability modulo yaw. The circles represent the initial condition of the simulator.

the extended Jacobian matrices. Since, the orbit is already stabilized modulo yaw, we only let $\Delta\xi$ parameterizes the first column of the H^{R} matrix which corresponds to the yaw position. Next, the optimization problem (47) is solved with $w_1 = 1$ and $w_2 = 0$. The optimal perturbation in the controlled variables is then given by

$$\begin{bmatrix} 0.0263\, q_{z\mathrm{T}} \\ 0.0230\, q_{z\mathrm{T}} \\ -0.0112\, q_{z\mathrm{T}} \\ -0.0186\, q_{z\mathrm{T}} \\ -0.0729\, q_{z\mathrm{T}} \\ 0.1065\, q_{z\mathrm{T}} \end{bmatrix}$$

for which the dominant eigenvalues of the estimated and real Jacobian matrices become $\{-0.8836 \pm 0.0529i, 0.8694 \pm 0.1051i, -0.1109\}$ and $\{-0.8854, -0.8854, 0.8757, 0.8757, -0.1109\}$, respectively. Figure 12 illustrates the phase portraits of the closed-loop system corresponding to the optimal solution during 80 consecutive steps of walking. During the fourth step, an external horizontal force with a magnitude of $70(\mathrm{N})$ is applied to the side of the robot to its COM over 50% of the step. Finally, Fig. 13 depicts the trajectory of the COM and the foot step locations in the xy-plane of the world frame. Convergence to the periodic orbit even in the yaw position is clear.

Other Nominal Output Functions To demonstrate the power of the sensitivity and BMI approach, we study the stabilization of other nominal output functions. We start with nominal controlled variables as in (70) in which the sixth component is replaced by

$$\frac{\partial}{\partial q}\left(\frac{1}{2}x_{\mathrm{sw}} - x_{\mathrm{COM}}\right)(x_f^*)\, q \tag{72}$$

where $\frac{1}{2}x_{\mathrm{sw}}(q) - x_{\mathrm{COM}}(q)$ represents the distance between the COM and the point midway between the the leg ends in the frontal plane[13]. In (72), the distance function has been linearized around the orbit $\mathcal{O}_{\mathrm{R}}$ just before the impact.

[13]The expression (72) assumes that the stance leg end is on the origin of the world frame.

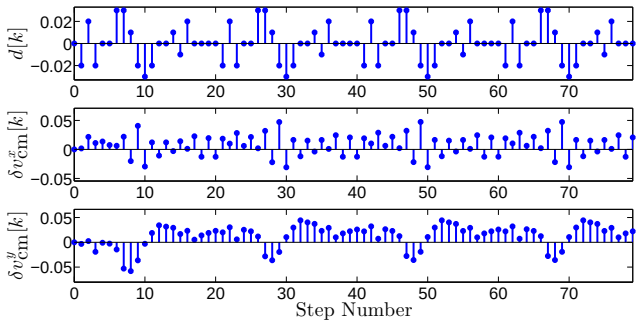

Fig. 10. Plot of the ground height profile $d[k]$ (m) and the corresponding x and y components of the deviation in ATRIAS's COM velocity (i.e., $\delta v_{\rm cm}[k]$) (m/s) for the optimal solution of (47) versus the step number k.

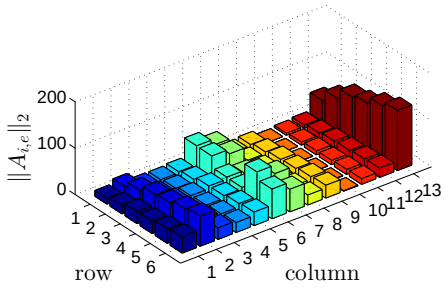

Fig. 11. Plot of the 2-norm of the extended sensitivity matrices versus the components of the 6×13 $H^{\rm R}$ matrix around the improved nominal output function (71).

The dominant eigenvalues of the Jacobian of the half Poincaré map are $\{-1.0000, 1.0499, -0.8455, 0.8430, -0.1130\}$ and hence, zeroing the output function cannot stabilize the orbit $\mathcal{O}$. The optimization problem (31) is then solved for exponential stability modulo yaw. The dominant eigenvalues of the Jacobian of the half Poincaré map based on the linear approximation of (21) are $\{-1.0000, -0.8702, 0.8359 \pm 0.0851i, -0.1329\}$. Next, the dominant eigenvalues of the real Jacobian of the half Poincaré map corresponding to this perturbation become $\{-1.0000, -0.8623, 0.8630 \pm 0.0713i, -0.1465\}$.

If the sixth component of the nominal controlled variables in (70) is defined as the swing hip angle $q_{3\rm L}$, the periodic orbit $\mathcal{O}$ is extremely unstable and the dominant eigenvalues of the Jacobian of the half Poincaré map are $\{-1.0000, -2.4587, 0.8414, -0.4228\}$. Next, for exponential stability modulo yaw, the optimization problem (31) is solved. The optimal perturbation values are then plugged in the output functions. However, the values are not small enough to have a good approximation based on the Taylor series expansion and as a consequence, the orbit $\mathcal{O}$ is not stable. In particular, the dominant eigenvalues of the real Jacobian of the half Poincaré map become $\{-1.0000, -1.2608, 0.8087, -0.2036\}$. Next, an alternative sensitivity analysis is done around the resultant perturbed output function. The optimal solution of (31) is then calculated. Finally, the dominant eigenvalues of Jacobian of the half Poincaré map, based on Taylor series expansion (21) and real calculations, are $\{-1.0000, -0.8561, 0.8418 \pm 0.1030i, -0.1084\}$ and $\{-1.0000, -0.8764, 0.7773 \pm 0.1056i, -0.1308\}$, respectively.

7. Conclusion

This paper introduced a method for designing continuous-time controllers to robustly and exponentially stabilize periodic orbits for hybrid systems. In contrast with previous methods that rely on recomputing the Jacobian of the Poincaré map at each step of a nonlinear optimization, the proposed method employs a sensitivity analysis to approximate the Jacobian

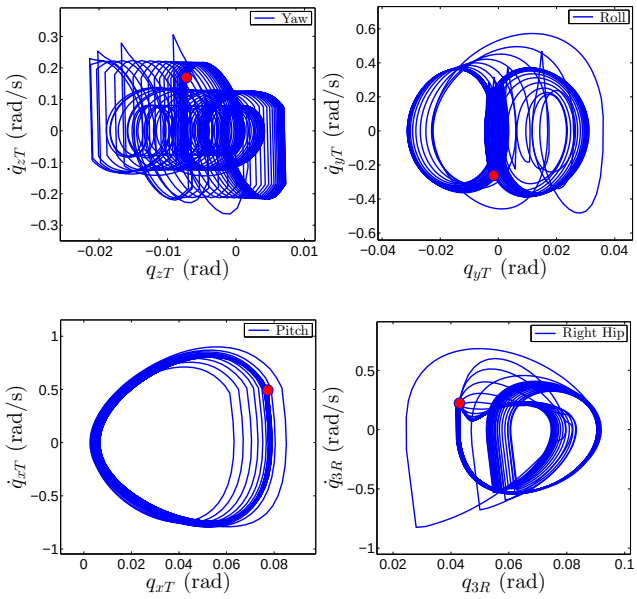

Fig. 12. Phase portraits of the closed-loop hybrid system for the Euler angles and right hip during 80 consecutive steps corresponding to the optimal solutions of (47) for full stability. The circles represent the initial condition of the simulator.

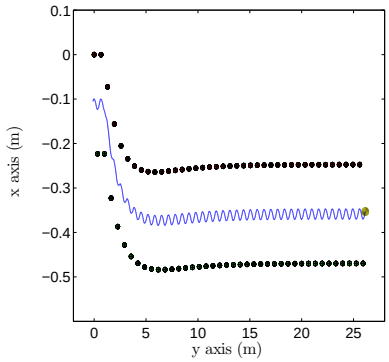

Fig. 13. Trajectory of the COM and feet trace during 80 consecutive steps of walking with yaw stability.

by an affine function of the control parameters. The resulting optimization problem involves LMI and BMI constraints and can be solved efficiently with existing software packages. The power of this approach was illustrated in the design of robust and stabilizing virtual constraints for two underactuated 3D bipedal robots with 8 and 13 DOF. The approach can handle both full-state stability and stability modulo yaw.

The algorithm presented in this paper can be extended to more general form of robust stabilization problems, including robustness against uncertainties rising from external forces acting on the robot. In future research, we will investigate these forms of uncertainties. We will also investigate the results for stable and 3D underactuated running by ATRIAS with 32 states and 6 actuators. Furthermore, the BMI optimization of this paper can be extended to improve stability of bipedal walking by designing proper phasing variables.

A. Proof of Lemma 1

Let us define the sensitivity of the solution with respect to the parameter vector as $\Psi(t, x_0, \xi) := \frac{\partial \varphi}{\partial \xi}(t, x_0, \xi) \in \mathbb{R}^{(n+1)\times p}$. From the definition of the solution $\varphi(t, x_0, \xi)$,

$$\varphi(t, x_0, \xi) = x_0 + \int_0^t f^{\mathrm{cl}}\left(\varphi(\tau, x_0, \xi), \xi\right) \mathrm{d}\tau. \tag{73}$$

Differentiating both sides of (73) with respect ξ and next with respect to the time yields the following matrix differential equation

$$\begin{aligned} \dot{\Psi}(t, x_0, \xi) = &\left.\frac{\partial f^{\mathrm{cl}}}{\partial x}(x, \xi)\right|_{x=\varphi(t,x_0,\xi)} \Psi(t, x_0, \xi) \\ &+ \left.\frac{\partial f^{\mathrm{cl}}}{\partial \xi}(x, \xi)\right|_{x=\varphi(t,x_0,\xi)} \\ \Psi(0, x_0, \xi) = &\, 0. \end{aligned} \tag{74}$$

Since f^{cl} is $\mathcal{C}^\infty$, the solutions of (74) are unique over the maximal interval of existence. Consequently, $\Psi(t, x_0, \xi) \equiv 0$ if and only if $\frac{\partial f^{\mathrm{cl}}}{\partial \xi}(x, \xi) = 0$ for all $x = \varphi(t, x_0, \xi)$.

B. Proof of Theorem 2

According to Items 2 and 3 of Assumption 1, $T(x_0^*, \xi) = T^*$ and $\Delta(x_f^*, \xi) = x_0^*$ for all $\xi \in \Xi$. This fact together with (17) implies that the Jacobian of the Poincaré return map can be expressed as[14]

$$\begin{aligned} \mathrm{D}_1 P(x_f^*, \xi) = &\, \mathrm{D}_1 \varphi(T^*, x_0^*, \xi)\, \mathrm{D}_1 T(x_0^*, \xi)\, \mathrm{D}_1 \Delta(x_f^*, \xi) \\ &+ \mathrm{D}_2 \varphi(T^*, x_0^*, \xi)\, \mathrm{D}_1 \Delta(x_f^*, \xi). \end{aligned} \tag{75}$$

Furthermore,

$$\begin{aligned} \mathrm{D}_1 \varphi(T^*, x_0^*, \xi) &= \dot{\varphi}(T^*, x_0^*, \xi) \\ &= f^{\mathrm{cl}}\left(\varphi(T^*, x_0^*, \xi), \xi\right) \\ &= f^{\mathrm{cl}}(x_f^*, \xi) \\ &= f^{\mathrm{cl}}(x_f^*, \xi^*), \end{aligned} \tag{76}$$

in which we have made use of the invariance condition (see (11)) in the last equality. $\mathrm{D}_2 \varphi(T^*, x_0^*, \xi)$ can also be expressed as

$$\begin{aligned} \mathrm{D}_2 \varphi(T^*, x_0^*, \xi) &= \frac{\partial \varphi}{\partial x_0}(T^*, x_0^*, \xi) \\ &= \Phi(T^*, x_0^*, \xi) \\ &= \Phi_f^*(\xi). \end{aligned} \tag{77}$$

[14] Following common convention for the partial derivatives of a $\mathcal{C}^1$ function $\rho(x_1, \cdots, x_v)$,

$$\mathrm{D}_j \rho(x_1, \cdots, x_v) := \frac{\partial \rho}{\partial x_j}(x_1, \cdots, x_v), \quad j = 1, \cdots, v.$$

From the switching and invariance conditions (see Item 2 of Assumption 1),

$$s(\varphi(T^*, x_0^*, \xi)) = 0, \quad \forall \xi \in \Xi$$

which together with the Implicit Function Theorem implies that

$$s(\varphi(T(x,\xi), x, \xi)) = 0 \tag{78}$$

for all x in an open neighborhood of x_0^* and all $\xi \in \Xi$. Differentiating (78) with respect to x around (x_0^*, ξ) results in

$$\begin{aligned} \mathrm{D}\, s(x_f^*)\, \mathrm{D}_1\, \varphi(T^*, x_0^*, \xi)\, \mathrm{D}_1\, T(x_0^*, \xi) \\ + \mathrm{D}\, s(x_f^*)\, \mathrm{D}_2\, \varphi(T^*, x_0^*, \xi) = 0 \end{aligned}$$

which in combination with (76), (77) and the transversality assumption results in

$$\mathrm{D}_1\, T(x_0^*, \xi) = -\frac{\frac{\partial s}{\partial x}(x_f^*)\, \Phi_f^*(\xi)}{\frac{\partial s}{\partial x}(x_f^*)\, f^{\mathrm{cl}}(x_f^*, \xi^*)}. \tag{79}$$

In particular, the Jacobian of the time-to-reset function depends on ξ only through $\Phi_f^*(\xi)$. Replacing (79) in (75) yields (48), from which (49) follows immediately.

C. Proof of Theorem 3

The proof of (52) is immediate from (37). To extract (54), from Assumption 1, $T_e(x_0^*, \xi, 0) = T^*$ for all $\xi \in \Xi$. Furthermore, the Implicit Function Theorem is applied to

$$s\left(\varphi\left(T_e(x,\xi,d), x, \xi\right)\right) = d \tag{80}$$

from which, it can be concluded that

$$\mathrm{D}\, s(x_f^*)\, \mathrm{D}_1\, \varphi(T^*, x_0^*, \xi)\, \mathrm{D}_3\, T_e(x_0^*, \xi, 0) - 1 = 0.$$

This latter equation together with (76) results in

$$\mathrm{D}_3\, T_e(x_0^*, \xi, 0) = \frac{1}{\frac{\partial s}{\partial x}(x_f^*)\, f^{\mathrm{cl}}(x_f^*, \xi^*)}. \tag{81}$$

Finally, P_e depends on d only through the extended time-to-reset function T_e (see (34)), and hence,

$$\mathrm{D}_3\, P_e(x_f^*, \xi, 0) = \mathrm{D}_1\, \varphi(T^*, x_0^*, \xi)\, \mathrm{D}_3\, T_e(x_0^*, \xi, 0).$$

This together with (81) and (76) completes the proof.

D. Numerical Calculation of the Sensitivity of the Reset Map Jacobian

The objective of this appendix is to investigate Item 3 of Assumption 1 for the hybrid model of 3D walking in (56). This section also provides a systematic approach to numerically calculate the sensitivity of the reset map Jacobian, i.e., $\frac{\partial \Upsilon}{\partial \xi_i}(x_f^*, \xi^*)$, where $\Upsilon(x_f^*, \xi) := \frac{\partial \Delta}{\partial x}(x_f^*, \xi)$ was already defined in Theorem 2.

Theorem 5 (Sensitivity of the Reset Map Jacobian)**.** *Let $\mathcal{O} = \mathcal{O}_R \cup \mathcal{O}_L$ be a transversal periodic orbit for the closed-loop hybrid model of 3D walking. Then the following statements are correct.*

1. *Items 1 and 3 of Assumption 1 are satisfied if*

$$\frac{\partial f_i^{cl}}{\partial \xi^i}(x, \xi^i)\Big|_{x \in \overline{\mathcal{O}}_i} = 0, \quad i \in \{R,L\}.$$

2. *Let $\{x_{f,R}^*\} := \overline{\mathcal{O}}_R \cap \mathcal{S}_{R\to L}$, $\{x_{f,L}^*\} := \overline{\mathcal{O}}_L \cap \mathcal{S}_{L\to R}$, and $x_f^* := x_{f,R}^*$. Suppose further that ξ^* denotes the nominal full parameter vector. Then, $\frac{\partial \Upsilon}{\partial \xi_i}(x_f^*, \xi^*), i = 1, \cdots, p$ in* (49) *can be expressed as*

$$\frac{\partial \Upsilon}{\partial \xi_i}(x_f^*, \xi^*) = \frac{\partial \Delta_{L\to R}}{\partial x}(x_{f,L}^*)\, \frac{\partial^2 P_{R\to L}}{\partial \xi_i \partial x}(x_{f,R}^*, \xi^*),$$

in which

$$\begin{aligned} \frac{\partial^2 P_{R\to L}}{\partial \xi_i \partial x}(x_{f,R}^*, \xi^*) &= \Pi_L(x_{f,L}^*, \xi^*)\, \frac{\partial \Phi_{f,L}^*}{\partial \xi_i}(\xi^*)\, \frac{\partial \Delta_{R\to L}}{\partial x}(x_{f,R}^*) \\ \Pi_L(x_{f,L}^*, \xi^*) &:= I_{(n+1)\times(n+1)} - \frac{f_L^{cl}(x_{f,L}^*, \xi^*)\, \frac{\partial s_{L\to R}}{\partial x}(x_{f,L}^*)}{\frac{\partial s_{L\to R}}{\partial x}(x_{f,L}^*)\, f_L^{cl}(x_{f,L}^*, \xi^*)} \end{aligned}$$

and $\Phi_{f,L}^*(\xi)$ denotes the final value of the trajectory sensitivity matrix $\Phi_L(t, x_0, \xi) := \frac{\partial \varphi_L}{\partial x_0}(t, x_0, \xi)$ on the orbit $\overline{\mathcal{O}}_L$.

Proof. According to (11), $\frac{\partial f_R^{\mathrm{cl}}}{\partial \xi^{\mathrm{R}}}(x, \xi^{\mathrm{R}}) = 0$ for all $x \in \overline{\mathcal{O}}_{\mathrm{R}}$ follows Item 1 of Assumption 1. In an analogous manner, $\frac{\partial f_L^{\mathrm{cl}}}{\partial \xi^{\mathrm{L}}}(x, \xi^{\mathrm{L}}) = 0$ for all $x \in \overline{\mathcal{O}}_{\mathrm{L}}$ results in $\frac{\partial \varphi_L}{\partial \xi^{\mathrm{L}}}(t, \Delta_{\mathrm{R}\to\mathrm{L}}(x_{f,\mathrm{R}}^*), \xi^{\mathrm{L}}) = 0$ for all $t \geq 0$, and hence,

$$P_{\mathrm{R}\to\mathrm{L}}(x_{f,\mathrm{R}}^*, \xi^{\mathrm{L}}) = x_{f,\mathrm{L}}^*, \quad \forall \xi^{\mathrm{L}} \in \Xi^{\mathrm{L}}.$$

This together with (58) completes the proof of Item 3 of Assumption 1. The proof of Part 2 is similar to the one presented in Theorem 2. □

Acknowledgments

B. G. Buss was supported by NSF Graduate Student Research Fellowship under Grant No. DGE 1256260. K. Akbari Hamed and J. W. Grizzle were supported by NSF Grants ECCS-1343720 and ECCS-1231171.

References

Akbari Hamed, K., Buss, B., and Grizzle, J. (2014). Continuous-time controllers for stabilizing periodic orbits of hybrid systems: Application to an underactuated 3d bipedal robot. In *IEEE Conference on Decision and Control, accepted to appear*.

Akbari Hamed, K. and Grizzle, J. (2014). Event-based stabilization of periodic orbits for underactuated 3-d bipedal robots with left-right symmetry. *Robotics, IEEE Transactions on*, 30(2):365–381.

Akbari Hamed, K., Sadati, N., Gruver, W., and Dumont, G. (2012). Stabilization of periodic orbits for planar walking with non-instantaneous double-support phase. *Systems, Man and Cybernetics, Part A: Systems and Humans, IEEE Transactions on*, 42(3):685–706.

Ames, A. (2014). Human-inspired control of bipedal walking robots. *Automatic Control, IEEE Transactions on*, 59(5):1115–1130.

Ames, A., Galloway, K., Sreenath, K., and Grizzle, J. (2014). Rapidly exponentially stabilizing control lyapunov functions and hybrid zero dynamics. *Automatic Control, IEEE Transactions on*, 59(4):876–891.

Ames, A., Gregg, R., and Spong, M. (2007). A geometric approach to three-dimensional hipped bipedal robotic walking. In *Decision and Control, 46th IEEE Conference on*, pages 5123–5130.

Ames, A. D., Sinnet, R. W., and Wendel, E. D. (2009). Three-dimensional kneed bipedal walking: A hybrid geometric approach. In Majumdar, R. and Tabuada, P., editors, *Hybrid Systems: Computation and Control*, volume 5469 of *Lecture Notes in Computer Science*, pages 16–30. Springer Berlin Heidelberg.

Arnold, V. (1996). *Geometrical Methods in the Theory of Ordinary Differential Equations*. Springer; 2nd edition.

ATRIAS (2013). `https://sites.google.com/site/atrias21/`.

Bainov, D. and Simeonov, P. (1989). *Systems With Impulse Effect: Stability, Theory and Applications*. Ellis Horwood Ltd.

Chevallereau, C., Abba, G., Aoustin, Y., Plestan, F., Westervelt, E., Canudas-de Wit, C., and Grizzle, J. (2003). Rabbit: a testbed for advanced control theory. *Control Systems, IEEE*, 23(5):57–79.

Chevallereau, C., Grizzle, J., and Shih, C.-L. (2009). Asymptotically stable walking of a five-link underactuated 3-d bipedal robot. *Robotics, IEEE Transactions on*, 25(1):37–50.

Dai, H. and Tedrake, R. (2012). Optimizing robust limit cycles for legged locomotion on unknown terrain. In *Decision and Control, IEEE 51st Annual Conference on*, pages 1207–1213.

Diehl, M., Mombaur, K., and Noll, D. (2009). Stability optimization of hybrid periodic systems via a smooth criterion. *Automatic Control, IEEE Transactions on*, 54(8):1875–1880.

Freidovich, L., Mettin, U., Shiriaev, A., and Spong, M. (2009). A passive 2-dof walker: Hunting for gaits using virtual holonomic constraints. *Robotics, IEEE Transactions on*, 25(5):1202–1208.

Goebel, R., Sanfelice, R., and Teel, A. (2012). *Hybrid Dynamical Systems: Modeling, Stability, and Robustness*. Princeton University Press.

Gregg, R., Lenzi, T., Hargrove, L., and Sensinger, J. (2014). Virtual constraint control of a powered prosthetic leg: From simulation to experiments with transfemoral amputees. *Robotics, IEEE Transactions on*, 30(6):1455–1471.

Gregg, R. and Sensinger, J. (2014). Towards biomimetic virtual constraint control of a powered prosthetic leg. *Control Systems Technology, IEEE Transactions on*, 22(1):246–254.

Gregg, R. and Spong, M. (2008). Reduction-based control with application to three-dimensional bipedal walking robots. In *American Control Conference*, pages 880–887.

Gregg, R., Tilton, A., Candido, S., Bretl, T., and Spong, M. (2012). Control and planning of 3-d dynamic walking with asymptotically stable gait primitives. *Robotics, IEEE Transactions on*, 28(6):1415–1423.

Griffin, B. and Grizzle, J. (2014). Walking gait optimization for accommodation of unknown terrain height variations. In *American Control Conference, submitted*.

Grimes, J. and Hurst, J. (2012). The design of atrias 1.0 a unique monoped, hopping robot. In *Climbing and Walking Robots and the Support Technologies for Mobile Machines, 2012 International Conference on*, pages 548–554.

Grizzle (2015). `http://web.eecs.umich.edu/~grizzle/papers/robotics.html`.

Grizzle, J., Abba, G., and Plestan, F. (2001). Asymptotically stable walking for biped robots: analysis via systems with impulse effects. *Automatic Control, IEEE Transactions on*, 46(1):51–64.

Grizzle, J. W. (2006). Remarks on event-based stabilization of periodic orbits in systems with impulse effects. In *Second International Symposium on Communication, Control and Signal Processing*.

Grizzle, J. W., Chevallereau, C., Sinnet, R. W., and Ames, A. D. (2014). Models, feedback control, and open problems of 3d bipedal robotic walking. *Automatica*, 50(8):1955–1988.

Haddad, W. and Chellaboina, V. (2008). *Nonlinear Dynamical Systems and Control: A Lyapunov-Based Approach*. Princeton University Press.

Haddad, W., Chellaboina, V., and Nersesov, S. (2006). *Impulsive and Hybrid Dynamical Systems: Stability, Dissipativity, and Control*. Princeton University Press.

Henrion, D., Lofberg, J., Kocvara, M., and Stingl, M. (2005). Solving polynomial static output feedback problems with penbmi. In *Decision and Control, and European Control Conference. 44th IEEE Conference on*, pages 7581–7586.

Hiskens, I. and Pai, M. (2000). Hybrid systems view of power system modelling. In *Circuits and Systems. Proceedings The 2000 IEEE International Symposium on*, volume 2, pages 228–231 vol.2.

Hobbelen, D. and Wisse, M. (2007). A disturbance rejection measure for limit cycle walkers: The gait sensitivity norm. *Robotics, IEEE Transactions on*, 23(6):1213–1224.

Holm, J., Lee, D., and Spong, M. (2007). Time-scaling trajectories of passive-dynamic bipedal robots. In *Robotics and Automation, IEEE International Conference on*, pages 3603–3608.

Hurmuzlu, Y. and Marghitu, D. B. (1994). Rigid body collisions of planar kinematic chains with multiple contact points. *The International Journal of Robotics Research*, 13(1):82–92.

Isidori, A. (1995). *Nonlinear Control Systems*. Springer; 3rd edition.

Lack, J., Powell, M., and Ames, A. (2014). Planar multi-contact bipedal walking using hybrid zero dynamics. In *Robotics and Automation, IEEE International Conference on*, pages 2582–2588.

Lofberg, J. (2004). Yalmip : a toolbox for modeling and optimization in matlab. In *Computer Aided Control Systems Design, 2004 IEEE International Symposium on*, pages 284–289.

Maggiore, M. and Consolini, L. (2013). Virtual holonomic constraints for euler lagrange systems. *Automatic Control, IEEE Transactions on*, 58(4):1001–1008.

Manchester, I. R., Mettin, U., Iida, F., and Tedrake, R. (2011). Stable dynamic walking over uneven terrain. *The International Journal of Robotics Research*, 30(3):265–279.

Martin, A. E. and Schmiedeler, J. P. (2014). Predicting human walking gaits with a simple planar model. *Journal of Biomechanics*, 47(6):1416–1421.

Morris, B. and Grizzle, J. (2009). Hybrid invariant manifolds in systems with impulse effects with application to periodic locomotion in bipedal robots. *Automatic Control, IEEE Transactions on*, 54(8):1751–1764.

Parker, T. and Chua, L. (1989). *Practical Numerical Algorithms for Chaotic Systems*. Springer.

Ramezani, A., Hurst, J., Akbai Hamed, K., and Grizzle, J. (2013). Performance analysis and feedback control of atrias, a three-dimensional bipedal robot. *Journal of Dynamic Systems, Measurement, and Control December, ASME*, 136(2).

Saglam, C. and Byl, K. (2013). Switching policies for metastable walking. In *Decision and Control, IEEE 52nd Annual Conference on*, pages 977–983.

Shih, C.-L., Grizzle, J. W., and Chevallereau, C. (2012). From stable walking to steering of a 3d bipedal robot with passive point feet. *Robotica*, 30:1119–1130.

Shiriaev, A., Freidovich, L., and Gusev, S. (2010). Transverse linearization for controlled mechanical systems with several passive degrees of freedom. *Automatic Control, IEEE Transactions on*, 55(4):893–906.

Shiriaev, A., Sandberg, A., and Canudas de Wit, C. (2004). Motion planning and feedback stabilization of periodic orbits for an acrobot. In *Decision and Control. 43rd IEEE Conference on*, volume 1, pages 290–295 Vol.1.

Spong, M. and Bullo, F. (2005). Controlled symmetries and passive walking. *Automatic Control, IEEE Transactions on*, 50(7):1025–1031.

Sreenath, K., Park, H.-W., Poulakakis, I., and Grizzle, J. (2013). Embedding active force control within the compliant hybrid zero dynamics to achieve stable, fast running on mabel. *The International Journal of Robotics Research*, 32(3):324–345.

Sreenath, K., Park, H.-W., Poulakakis, I., and Grizzle, J. W. (2011). Compliant hybrid zero dynamics controller for achieving stable, efficient and fast bipedal walking on MABEL. *The International Journal of Robotics Research*, 30(9):1170–1193.

Tedrake, R., Zhang, T., and Seung, H. (2004). Stochastic policy gradient reinforcement learning on a simple 3d biped. In *Intelligent Robots and Systems. Proceedings 2004 IEEE/RSJ International Conference on*, volume 3, pages 2849–2854 vol.3.

Toker, O. and Ozbay, H. (1995). On the np-hardness of solving bilinear matrix inequalities and simultaneous stabilization with static output feedback. In *American Control Conference, Proceedings of the 1995*, volume 4, pages 2525–2526 vol.4.

TOMLAB (2015). `http://tomopt.com/tomlab/`.

VanAntwerp, J. and Braatz, R. (2000). A tutorial on linear and bilinear matrix inequalities. *Journal of Process Control*, 10(4):363–385.

Westervelt, E., Grizzle, J., Chevallereau, C., Choi, J., and Morris, B. (2007). *Feedback Control of Dynamic Bipedal Robot Locomotion*. Taylor & Francis/CRC.

Westervelt, E., Grizzle, J., and Koditschek, D. (2003). Hybrid zero dynamics of planar biped walkers. *Automatic Control, IEEE*

Transactions on, 48(1):42–56.

Ye, H., Michel, A., and Hou, L. (1998). Stability theory for hybrid dynamical systems. *Automatic Control, IEEE Transactions on*, 43(4):461–474.